HHS Public Access

Author manuscript

Cell Rep. Author manuscript; available in PMC 2021 May 06.

Published in final edited form as:

Cell Rep. 2021 January 12; 34(2): 108620. doi:10.1016/j.celrep.2020.108620.

Targeting Phosphatidylserine Enhances the Anti-tumor Response to Tumor-Directed Radiation Therapy in a Preclinical Model of Melanoma

Sadna Budhu[1], **Rachel Giese**[1,2], **Aditi Gupta**[1,3], **Kelly Fitzgerald**[1,4], **Roberta Zappasodi**[1,3], **Sara Schad**[1,3], **Daniel Hirschhorn**[1], **Luis Felipe Campesato**[1], **Olivier De Henau**[1], **Mathieu Gigoux**[1], **Cailian Liu**[1], **Gregory Mazo**[5,6], **Liang Deng**[3,5,6], **Christopher A. Barker**[4], **Jedd D. Wolchok**[1,3,5,7,*], **Taha Merghoub**[1,3,5,7,8,*]

[1]Swim Across America and Ludwig Collaborative Laboratory, Immunology Program, Parker Institute for Cancer Immunotherapy at Memorial Sloan Kettering Cancer Center, New York, NY 10065, USA

[2]Department of Surgery, Memorial Sloan Kettering Cancer Center, New York, NY 10065, USA

[3]Weill Cornell Medical College, New York, NY 10065, USA

[4]Department of Radiation Oncology, Memorial Sloan Kettering Cancer Center, New York, NY 10065, USA

[5]Department of Medicine, Memorial Sloan Kettering Cancer Center, New York, NY 10065, USA

[6]Dermatology Service, Memorial Sloan Kettering Cancer Center, New York, NY 10065, USA

[7]Human Oncology and Pathogenesis Program, Memorial Sloan Kettering Cancer Center, New York, NY 10065, USA

[8]Lead Contact

SUMMARY

Phosphatidylserine (PS) is exposed on the surface of apoptotic cells and is known to promote immunosuppressive signals in the tumor microenvironment (TME). Antibodies that block PS interaction with its receptors have been shown to repolarize the TME into a proinflammatory state. Radiation therapy (RT) is an effective focal treatment of isolated solid tumors but is less effective at controlling metastatic cancers. We found that tumor-directed RT caused an increase in expression of PS on the surface of viable immune infiltrates in mouse B16 melanoma. We hypothesize that PS expression on immune cells may provide negative feedback to immune cells in the TME. Treatment with an antibody that targets PS (mch1N11) enhanced the anti-tumor

*Correspondence: wolchokj@mskcc.org (J.D.W.), merghout@mskcc.org (T.M.).

AUTHOR CONTRIBUTIONS

Conceptualization: S.B., C.A.B., T.M., and J.D.W.; Methodology: S.B., R.Z., S.S., D.H., M.G., C.L., G.M., L.D., and C.A.B.; Investigation & Resources: R.G., A.G., K.F., R.Z., O.D., S.S., D.H., L.F.C., M.G., C.L., G.M., L.D., and C.A.B.; Formal Analysis: S.B.; Visualization: S.B.; Writing – Original Draft: S.B.; Writing – Review & Editing: R.G., L.F.C., M.G., C.A.B., T.M., and J.D.W.; Supervision & Funding Acquisition: T.M. and J.D.W.

SUPPLEMENTAL INFORMATION

Supplemental Information can be found online at https://doi.org/10.1016/j.celrep.2020.108620.

efficacy of tumor-directed RT and improved overall survival. This combination led to an increase in proinflammatory tumor-associated macrophages. The addition of anti-PD-1 to RT and mch1N11 led to even greater anti-tumor efficacy and overall survival. We found increased PS expression on several immune subsets in the blood of patients with metastatic melanoma after receiving tumor-directed RT. These findings highlight the potential of combining PS targeting with RT and PD-1 pathway blockade to improve outcomes in patients with advanced-stage cancers.

In Brief

Budhu et al. show that tumor-directed irradiation of murine B16 melanoma causes an increase in PS on the surface of infiltrating immune cells. Blocking PS and RT improves the anti-tumor efficacy and overall survival, which can be further improved with the addition of anti-PD-1. Melanoma patients exhibit increased PS on their PBMCs after RT.

Graphical Abstract

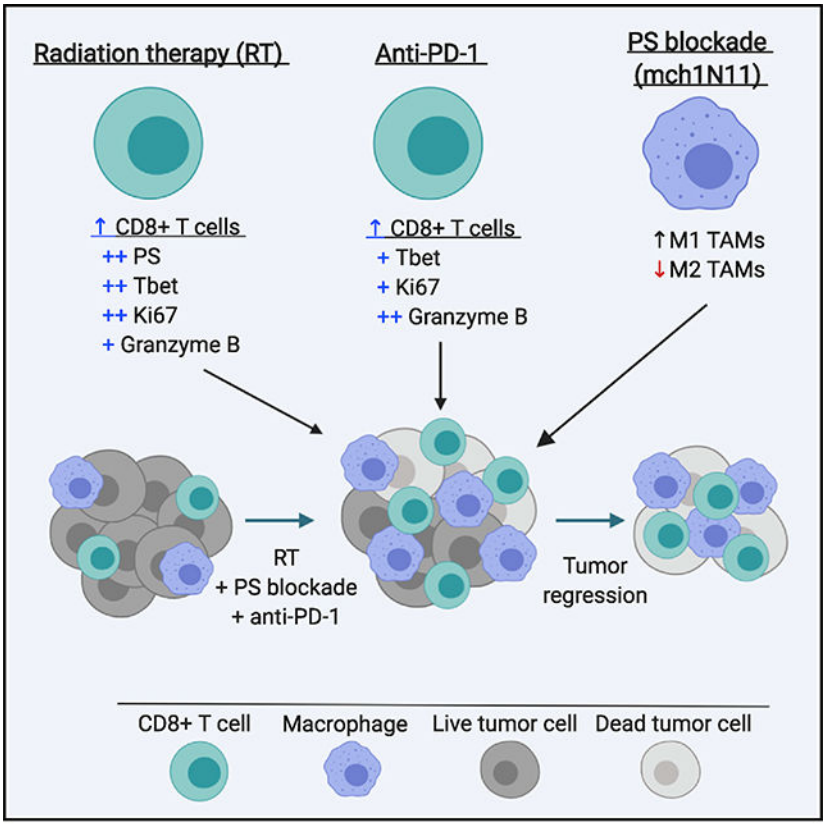

INTRODUCTION

Phosphatidylserine (PS) is a phospholipid normally found on the inner leaflet of the plasma membrane in healthy cells. Upon activation of certain downstream signals (e.g., caspase-3/7), enzymes such as scramblases can collapse the polarized distribution of PS, causing accumulation on the outer membrane (Birge et al., 2016). Cell surface expression of

PS is classically thought to be exclusive to apoptotic cells, in which externalized PS acts as an “eat me” signal for PS receptors expressed on macrophages and promotes clearance of apoptotic debris (efferocytosis). This process has been shown to be immunosuppressive in tissues because of attenuation of dendritic cell (DC) and natural killer (NK) cell activation and conversion of tumor-associated macrophages (TAMs) into anti-inflammatory or M2 macrophages (Graham et al., 2014; Kumar et al., 2017). Numerous PS receptors are ubiquitously expressed on immune cells. Among these are immunosuppressive receptors that belong to the Axl/Mer/Tyro3 receptor tyrosine kinase family, T cell immunoglobulin mucin domain (TIM) receptors, integrins, and the scavenger receptor family (Birge et al., 2016; Graham et al., 2014). Although some receptors directly bind to PS, other require an adaptor protein (e.g., GAS6) to bridge PS with its receptors.

PS can also be expressed on the surface of viable cells. PS is externalized on activated platelets, monocytes, mature macrophages, activated B cells, activated T cells, DCs, tumor vasculature, tumor cells, and the surface of exosomes derived from tumors (Birge et al., 2016). PS exposure on viable cells does not induce phagocytosis, because phagocytes are able to distinguish PS on viable versus apoptotic cells. The exact mechanism of this phenomenon remains unknown; however, PS exposure on apoptotic cells is caspase-3/7 dependent with slow kinetics (in hours) and is irreversible, whereas PS exposure on viable cells is thought to depend on intracellular Ca^{2+} with more rapid kinetics (in minutes) and is reversible (Birge et al., 2016). In addition, the density and spatial distribution of PS on the cell surface may dictate how phagocytic cells and their receptors distinguish dying from viable cells.

Several strategies have been developed to block PS interaction with its receptors (Belzile et al., 2018; Kumar et al., 2017; Sharma and Kanwar, 2018). These include an annexin V fusion protein, blocking antibodies that target PS and inhibitors of PS receptors. Monoclonal antibodies that block PS interactions with its receptors have demonstrated anti-tumor activity in mouse tumor models (He et al., 2009; Huang et al., 2005; Ran et al., 2005; Yin et al., 2013). These antibodies exert their anti-tumor effects through destruction of the tumor vasculature (He et al., 2009; Ran et al., 2005). In addition, they repolarized TAMs into a proinflammatory M1 phenotype, reduce the number of myeloid-derived suppressor cells (MDSCs) in tumors, and promote the maturation of DCs into functional antigen-presenting cells (APCs). In syngeneic mouse models of breast cancer and melanoma, targeting PS using the mouse monoclonal antibody mch1N11, which blocks the interaction of PS with its receptors, in combination with immune checkpoint blockade (ICB) promoted greater anti-tumor activity than either agent alone (Freimark et al., 2016; Gray et al., 2016).

Radiation therapy (RT) is commonly used for the treatment of cancer. The abscopal effect, a phenomenon in which tumor-directed radiation is associated with the regression at a distal site, has been observed with RT. However, the frequency of this occurrence is exceedingly low (Siva et al., 2015). RT can induce immunogenic tumor cell death, leading to efficient priming of tumor-antigen-specific T cell responses (Apetoh et al., 2007; Panaretakis et al., 2009). RT can also induce expression of proteins such as major histocompatibility complex (MHC) class I and intercellular adhesion molecule 1 (ICAM-1), which allows antigens presented by tumor cells to be better recognized, leading to more efficient elimination by

cytotoxic T cells (Gameiro et al., 2014). CD8+ T cells appear to be essential for the antitumor effects of RT (Chen et al., 2018; Gupta et al., 2012; Lee et al., 2009). When CD8+ T cells were depleted using monoclonal antibodies, there was an abrogation of the anti-tumor responses of RT (Gupta et al., 2012; Rodriguez-Ruiz et al., 2016). In addition, RT is associated with increased activation and infiltration of CD8+ T cells in tumors. This effect depends on type I interferons (IFNs) and is associated with the activation and recruitment of cross-presenting/Batf3-dependent DCs (Rodriguez-Ruiz et al., 2016; Vanpouille-Box et al., 2017).

Tumor-directed RT can enhance ICB by overcoming some resistance mechanisms associated with ICB. It can turn a poorly infiltrated “cold” tumor into a highly infiltrated “hot” tumor. Tumor-directed RT may act as an *in situ* vaccine, triggering activation of tumor-antigen-specific T cells (Lugade et al., 2005). It can also recruit activated CD4+ and CD8+ effector T cells to the tumor site via the release of chemokines and upregulation of adhesion molecules in tumor vasculature (Lugade et al., 2005; Matsumura et al., 2008). Several clinical reports on the abscopal effect in melanoma patients who received immunotherapy and tumor-directed RT have renewed interest in RT as a means to potentiate the efficacy of ICB (Golden et al., 2013; Hiniker et al., 2012; Okwan-Duodu et al., 2015; Postow et al., 2012; Stamell et al., 2013).

In this study, we show that PS expression on immune cells infiltrating mouse B16 melanoma was increased after a single dose of tumor-directed RT. We blocked PS signaling using the monoclonal antibody mch1N11 and showed that it enhanced the anti-tumor efficacy of tumor-directed RT. This combination enhanced priming of tumor-antigen-specific T cells and their recruitment to the tumor. In addition, there was a repolarization of the tumor microenvironment (TME) from an anti- to a proinflammatory state with the combination therapy. When ICB (anti-program cell death protein 1 [anti-PD-1]) was added to the combination of RT and PS blockade, there was an even greater delay of tumor growth and overall survival. This triple-combination therapy induced potent activation of cytotoxic CD8+ T cells in the tumor and the periphery, leading to enhanced abscopal responses in a contralateral (non-irradiated) tumor model. In agreement with the mouse studies, we show that immune subsets in the peripheral blood of melanoma patients exhibited an increase of PS expression 4–7 days after tumor-directed RT.

RESULTS

PS Expression on Immune Cell Subsets Increases after RT in the TME

We sought to carefully examine PS expression on immune cells in the TME. C57BL/6 mice were implanted with B16 melanoma cells intradermally, and tumors were harvested 10 days later to examine PS expression by flow cytometry. Because annexin V is commonly used to label PS on apoptotic cells, we co-stained for caspase-3/7 activity and a viability dye to distinguish PS expression on viable cells from apoptotic and dead cells (Figure 1A). Annexin V staining was compared with a PS antibody, which showed similar staining patterns on immune cells; however, annexin V staining exhibited better resolution than the PS antibody (Figure S1A). When gated on viable immune cells in the tumor, the annexin V+ single-positive cells are distinct from caspase-3/7+ or apoptotic cells (Figure 1B). Many

viable immune cell subsets in the tumor express PS on their surface (Figure 1C). This expression pattern varied considerably on different immune cell types, with myeloid cells expressing the highest amounts of PS. The expression pattern of PS on immune subsets in the tumor was confirmed using an anti-PS antibody (Figure S1B). Because RT is known to directly induce immunogenic cell death within the TME, we hypothesized that RT may increase cell surface PS expression on both tumor cells and immune infiltrates. To test this, we examined the expression of PS on these cells after tumor-directed RT. The right hindlimbs of C57BL/6 mice were implanted with B16 melanoma cells, and 10 days later, they were irradiated with a single dose of 15 Gy (Figure 1, schema). This dose and schedule of radiation were previously determined to exhibit optimal immune-stimulatory activity against B16 melanoma *in vivo* (Lugade et al., 2005). Tumors were excised 1, 5, and 10 days after RT and examined for expression of PS. No significant changes in frequencies or PS expression were observed on immune subsets at early time points (1 and 5 days post-RT) (Figure S1C). However, there was a marked increase in CD8+ T cells coupled with a decrease in myeloid cells 10 days after RT (Figure 1D). PS expression, on immune cells devoid of caspase activity, was increased 10 days after RT on nearly all cell types present in the tumor, with the greatest increase seen on the myeloid cells and the tumor cells (Figure 1E). Because RT is known to ablate immune cells in the TME, the observation that it takes 10 days to see an increase in PS expression may reflect the time it takes for these cells to be primed in the secondary lymphoid organs and then migrate to and repopulate the tumor. We also observed that B16F10 cells, when treated with 15 Gy RT *in vitro*, upregulated surface expression of PS within 24 h, demonstrating a direct effect of RT on PS expression on tumor cells (Figure S1D). This effect is enhanced with the addition of cytokines such as IFNγ to the culture. Because CD8+ T cells are a source for proinflammatory cytokines such as IFNγ, we asked whether CD8+ T cells were necessary for the increase in PS expression in the TME. We depleted CD8+ T cells using a depleting antibody (clone 2.43) starting the same day as RT and examined the expression PS in the TME 10 days later. Depletion was confirmed in the tumors on day 10 by flow cytometry (Figure S1E). CD8-depleted mice showed significantly diminished PS staining (annexin V+) on immune cells in the tumors 10 days after RT (Figure S1F). Tumor-directed RT is known to activate the c-GAS/Sting pathway, leading to the secretion of type I IFNs and maturation of DCs (Diamond et al., 2018). We tested whether the cyclic GMP-AMP Synthase (c-GAS)/Sting pathway was involved in the upregulation of PS using $Sting^{-/-}$ B16F10 cells and $Sting^{Gt/Gt}$ C57BL/6 mice (Sauer et al., 2011). The c-GAS/Sting pathway does not appear to be necessary for the observed increase in PS expression, because PS is significantly increased on immune cells in the TME of $Sting^{Gt/Gt}$ mice (Figure S1F). These results indicate that CD8+ T cells are partly responsible for the increase of PS expression on immune cells in tumors after RT. In addition, we observed similar increases in PS expression, albeit to a lesser extent, on immune subsets in the spleen at 10 days (but not 1 or 5 days) after RT, suggesting that this effect was systemic (Figure S1G).

Targeting PS in Combination with Tumor-Directed RT Enhances Anti-tumor Efficacy in B16 Melanoma

The finding that PS expression increased after RT in the TME suggests that PS may provide an inhibitory signal to immune cells that limits the immune-mediated anti-tumor efficacy of

RT. Because many schedules and doses of RT in preclinical and clinical settings are capable of controlling tumor growth but do not uniformly cure tumors, it is possible that PS expression is associated with acquired resistance to RT and may act similar to an immune checkpoint molecule to curtail immune responses. Hypothesizing that blocking PS on the surface of immune cells may help remove the immunosuppression and improve the anti-tumor efficiency of RT, we examined the effects of combining RT with PS blockade. To test this, we used a PS-targeting antibody, mch1N11, a mouse immunoglobulin G isotype 2a (IgG2a) chimeric version of the human PS-targeting antibody 1N11 (Mineo et al., 2016). This antibody does not directly bind PS but rather blocks its interaction with PS receptors (Belzile et al., 2018). We treated mice bearing B16 melanoma with a single dose of 15 Gy RT 10 days after implantation, and 1 day following RT, mice received mch1N11 (200 μg/mouse) via intraperitoneal (i.p.) injection, followed by a second dose 3 days later (Figure 2, schema). A single dose of 15 Gy was effective at controlling B16 tumor growth for approximately 2 weeks, after which 90% of tumors begin to regrow (Figure 2A). Treatment with mch1N11 alone had no significant effect on B16 tumor growth. However, there was greater anti-tumor efficacy in the animals treated with mch1N11 and RT, a setting in which 40% of the mice demonstrated complete regression of tumors. This combination led to significantly longer overall survival, with a median survival of 65 days with the combination versus 57 days with RT alone (Figures 2B and 2C).

Targeting PS with mch1N11 Promotes M1 Macrophage Polarization *In Vitro* and *In Vivo*

A PS-targeting antibody similar to mch1N11 has been previously shown to repolarize TAMs toward a proinflammatory M1 phenotype (Yin et al., 2013). We cultured bone-marrow-derived macrophages (BMDMs) in the presence of mch1N11 or an isotype-matched control (C44) for 24 h to examine whether this antibody can promote proinflammatory macrophages *in vitro*. The culture conditions to derive BMDMs generated primarily macrophages (CD11b + F4/80+ cells), which were the dominant cell population expressing PS (Figure 3A). Using the mannose receptor (CD206) and MHC class II expression to distinguish between M1 and M2 macrophages (Figure 3B), we found that mch1N11 decreased M2 macrophages (CD206+ MHC II−) and increased M1 macrophages (CD206− MHC II+) after 24 h in culture (Figure 3C). This led to a favorable skewing of the M1/M2 macrophage ratio, shifting the macrophage polarization to a proinflammatory phenotype. We next determined whether mch1N11 in combination with RT can repolarize TAMs *in vivo*. At an early time point (3 days post-treatment), there were no differences in the total TAM population or their polarization status in the treated groups (Figure 3D). At 10 days post-treatment, there was a significant increase in the frequency of TAMs in the tumors treated with RT or the combination with mch1N11. This increase appears to mainly result from RT alone. In addition, we observed a significant decrease in M2 macrophages and a corresponding increase in M1 macrophages in the combination treatment group. This resulted in an ~15-fold increase in the M1/M2 macrophage ratio in the tumor, significantly shifting the TAMs toward a proinflammatory phenotype (Figure 3E). In addition, we examined the frequencies of total APCs, which are phenotypically defined as CD11c+ MHC II+ cells and therefore represent a mixture of both TAMs and DCs, because subsets of both of these cell types express CD11c and MHC class II. We found an early increase in the frequencies of APCs that is only observed in the RT groups. However, no significant changes in APCs were

observed at later time points (Figures 3D and 3E). These data suggest that the combination of RT and mch1N11 exerts its effects on TAMs, but not on other populations of APCs.

Targeting PS in Combination with RT Promotes an Increase in Proinflammatory Cytokine Gene Expression and a Corresponding Decrease in Anti-inflammatory Genes

To better understand the effects of RT and mch1N11 on the TME, we isolated RNA from whole tumors 4 days after treatment and analyzed the expression of a preselected list of pro- and anti-inflammatory genes (Table S1). mch1N11 treatment alone showed a decrease in many pro- and anti-inflammatory genes, whereas RT alone led to an increase in expression of many proinflammatory cytokines (Figure 3F; Figure S2). The combination of RT and mch1N11 not only significantly increased expression of many proinflammatory cytokines but also decreased expression of anti-inflammatory markers such as CD206, transforming growth factor β (TGF-β), arginase 1, Foxp3, and interleukin (IL) 4-Rα (Figure 3F; Figure S2). When compared with RT alone, 2 genes—IL-2 and IFNβ—were significantly upregulated in the combination treatment group. These data suggest that RT alone and in combination with mch1N11 alter the transcriptional profile of cells in the TME to a proinflammatory microenvironment, with changes in both innate and adaptive immunity.

Targeting PS Enhances Tumor-Antigen-Specific T Cell Priming in Response to RT

RT has been shown to prime and recruit CD8+ T cells to tumors (Chen et al., 2018; Gupta et al., 2012; Lugade et al., 2005). The finding that the combination therapy repolarizes TAMs to become proinflammatory suggests that the TME is now more permissive to priming and activation of tumor-specific T cells. We investigated whether targeting PS in combination with tumor-directed RT had a systemic effect on T cell activation. We analyzed CD4+ and CD8+ T cells in the draining lymph nodes (LNs) 10 days after initial treatment. We found an increase in T cell activation markers such as Ki67 and CD25 in both CD4+ and CD8+ T cells (Figure S3A) and a significant increase in effector memory T cells (Figure 4A) in the combination treatment group. In addition, T cells in the combination group had higher expression of effector molecules, such as the cytolytic enzyme granzyme B and the proinflammatory cytokines IFNγ and tumor necrosis factor alpha (TNFα) (Figure 4A; Figure S3A). This led us to postulate that the combination of RT and mch1N11 leads to T cell priming in the draining LNs and spleen. To test this more definitively, we examined whether this therapy can enhance the priming of tumor-antigen-specific CD8+ T cells and their recruitment to the tumor site. We isolated naive CD8+ T cells from a transgenic mouse whose T cell receptor (TCR) specifically recognized a melanoma differentiation antigen gp100 (or Pmel-1), which is a tumor antigen in the case of melanoma (Overwijk et al., 2003). We adoptively transferred carboxyfluorescein succinimidyl ester (CFSE)-labeled naive tumor-antigen-specific Pmel CD8+ T cells into tumor-bearing animals treated with RT alone or RT in combination with mch1N11. Pmel CD8+ T cells were transferred on the same day as RT treatment, and the animals were given two doses of mch1N11 (Figure 4B, schema). Seven days following RT, blood, spleens, tumor-draining LNs, and tumors from the treated animals were isolated and analyzed for priming and activation of transferred Pmel CD8+ T cells. The congenic marker Thy1.1 expressed by Pmel CD8+ T cells was used to distinguish the transferred cells (Thy1.1+) from the endogenous CD8+ T cells (Thy1.1−) in these tissues (Figure 4B). The combination of RT with mch1N11 significantly increased the

frequency of tumor-antigen-specific T cell in all tissues (Figure 4C). Tumor-bearing mice that were untreated or treated with mch1N11 without RT were inefficient in priming Pmel CD8+ T cells (Figure 4C; data not shown). The transferred Pmel T cells proliferated efficiently (as measured by CFSE dilution) in response to RT and the combination treatment, with the greatest effects seen in tumor-draining LNs and tumors (Figures 4D and 4E). The numbers of transferred cells were relatively low in some tissues, making it difficult to analyze their activation status with statistical power. However, we did observe an overall increase in central memory and effector memory T cells, as well as an increase in PS expression on the surface of transferred T cells in all tissues examined in response to both RT and the combination (Figure S3B). In addition, examination of the endogenous CD8+ T cells in these tissues showed an increase in central memory and effector memory T cells and in surface PS expression, suggesting that there was effective priming of endogenous T cells in response to RT and the combination treatment (Figure S3B).

Anti-PD-1 Enhances the Anti-tumor Efficacy of RT and mch1N11

Because of the clinical success of immunotherapies targeting T cell checkpoints such as the cytotoxic T-lymphocyte-associated protein 4 (CTLA-4), PD-1 and its ligand (PD-L1), ICB is now a commonly used cancer treatment and the focus of clinical research. We asked whether ICB could enhance the therapeutic efficacy of the combination treatment and examined the effects of combining tumor-directed RT with mch1N11 and anti-PD-1. Our rationale for combining anti-PD-1 with RT and mch1N11 is 2-fold. First, we and others have observed that PD-L1 expression is increased on the surface of tumor cells after RT (Deng et al., 2014; Twyman-Saint Victor et al., 2015). We also found that PD-1 expression is increased on tumor-infiltrating CD8+ T cells with the combination of RT and anti-PS (Figure S3B). Therefore, because the ligand and receptor are present in the TME, activation of the PD-1/PD-L1 axis in T cells may limit the effectiveness of RT and mch1N11. Second, when thinking of the feasibility of translating our findings to the clinic, we must consider that PD-(L)1 blockade is becoming a standard approach for the treatment of various cancers, including melanoma. It would be challenging to design a clinical trial in which patients that are naive to immunotherapy can realistically be accrued with an experimental drug (e.g., bavituximab, the clinical equivalent of mch1N11) in lieu of anti-PD-(L)1. In our experimental setting (Figure 5, schema), anti-PD-1 is given using a suboptimal schedule, which shows a modest delay in tumor growth, and only ~10% of the animals have complete tumor regression (Figures 5A and 5B). Treatment of anti-PD-1 with mch1N11 further delayed tumor progression; however, the combination of these two agents with RT showed the greatest anti-tumor efficacy and overall survival (Figure 5). In the triple combination, 60% of the animals had complete regression of tumors compared with 30% with RT and mch1N11 and 40% with RT and anti-PD-1 (Figures 5A and 5B). In addition, median survival for the triple-combination group was >80 days compared with 65 days in the RT and mch1N11 or RT and anti-PD-1 groups (Figure 5C). These data suggest that the adding RT with a clinical PS-targeting agent (e.g., bavituximab) could potentially enhance clinical outcomes. The c-GAS/Sting pathway has been linked the anti-tumor response to RT (Diamond et al., 2018; Formenti et al., 2018). We explored the role of this pathway in the triple-combination therapy using $Sting^{-/-}$ B16F10 cells and Sting knockout (KO) mice ($Sting^{Gt/Gt}$). Activation of the Sting pathway may be important for the anti-tumor efficacy of

RT alone, because tumor growth control and median survival appear to be lower in the $Sting^{Gt/Gt}$ mice (Figure S4A). However, activation of the c-GAS/Sting pathway appears to be dispensable for the triple-combination therapy, in which tumor growth control, median survival, and overall survival do not appear to be significantly different in the wild-type (WT) versus KO groups.

We examined whether the triple-combination therapy can also be effective in a non-melanoma model. MC38 colon carcinoma is considered more immunogenic and more responsive to anti-PD-1 than B16 melanoma. C57BL/6 mice were implanted subcutaneously on the right hindlimb with MC38 cells, and tumors were treated with the same antibody dose and schedule as in the B16 experiments. We found that the therapies without radiation (anti-PD-1 alone and mch1N11 + anti-PD-1) showed similar results in delaying MC38 tumor growth when compared with B16 melanoma (Figure S4B versus Figures 5A and 5B). However, the overall survival was better in the combination of mch1N11 and anti-PD-1 for MC38 (Figure S4B). The addition of RT led to potent anti-tumor responses and overall survival in all RT groups, and 78%–100% of the mice had complete tumor regression. To determine whether these treatments conferred long-term immunity in the cured animals, we reimplanted 500,000 MC38 cells on the right flank 100 days after the first treatment. All cured animals were able to delay the secondary rechallenge equally, with an average of 40% of all treated groups (and 34% of the RT groups) remaining tumor free (Figure S4C).

Targeting PS in Combination with RT and Anti-PD-1 Promotes CD8+ T Cell Activation

A stringent test of any therapy that involves tumor-directed treatment (such as RT) is whether it can induce a systemic immune response. CD4+ and CD8+ T cells from the spleen and draining LNs of treated animals showed an increase in T cell activation markers such as Ki67 and granzyme B, with the greatest effects generally seen using the triple combination (Figures S5A and S5B). There were no changes in CD4+Foxp3+ regulatory T cells (Tregs) observed in the periphery. Recently, we described a suppressive population of CD4+ T cells that do not express the transcription factor Foxp3 but express high levels of PD-1 (Zappasodi et al., 2018a). We found that these CD4+ Foxp3− $PD\text{-}1^{hi}$ ($4PD\text{-}1^{hi}$) T cells are decreased in the spleen and LNs, leading to a corresponding increase in the ratio of CD8 and CD4 to $4PD\text{-}1^{hi}$ cells in both tissues (Figures S5C and S5D). In addition, we purified CD8+ T cells from the spleens of treated animals and conducted an *ex vivo* T cell killing assay using B16 cells as targets. We found that CD8+ T cells killed B16 tumor cells most efficiently in conditions in which mch1N111 was added to RT and/or anti-PD-1 (Figure 6A). Thus, it appears that treatment with mch1N11 promotes cytolytic T cells systemically. These data demonstrate that this triple-combination therapy induces a strong systemic immune response that may be capable of controlling distant tumors or metastases. Using a bilateral tumor model, we examined the effect of combining RT with mch1N11 and anti-PD-1 on secondary non-irradiated (abscopal) tumors (Figure 6B, schema). The combination of RT and anti-PD-1 and the triple combination of RT, mch1N11, and anti-PD-1 significantly reduced the growth of the secondary non-irradiated tumors, suggesting that these treatment regimens induce potent systemic anti-tumor responses (Figure 6B).

The observation that the triple combination of RT, mch1N11 and anti-PD-1 produced the most effective anti-tumor responses and overall survival prompted us to determine the impact of each of these therapies alone or in combination on the immune responses in the tumor. 10 days after treatment, anti-PD-1 alone or in combination with mch1N11 increased CD8+ T cell infiltration in the tumors from ~18% to ~40% of the total immune infiltrates within the treated tumors (Figure 6C). When RT was added, there was a greater increase in CD8+ T cell infiltration in the tumor with RT alone or in combination with mch1N11 and/or anti-PD-1. In all RT groups, the increase in CD8+ T cells accounted for ~60% of all immune cells (CD45+ cells) present in the tumor. The frequency of CD8+ T cells (relative to the total immune infiltrates in the tumor) had a strong inverse correlation with the tumor weight in all groups (Figure 6C). Moreover, the CD8+ T cells in the tumors were qualitatively different in each treatment group. In all groups that received tumor-directed RT, CD8+ T cells displayed increased expression of activation markers such as Ki67 and the transcription factor Tbet (Figure 6C). This effect was also observed in the combination of mch1N11 and anti-PD-1 without RT. In addition, there was an increase in CD8+ T cell expression of granzyme B in the combinations that included mch1N11 and anti-PD-1 (±RT). These T cell activation markers correlated inversely with tumor size, with the strongest correlation seen in the Tbet+ CD8+ T cells (Figure 6C). We also observed an increase in PD-1+ CD8+ T cells in all RT groups. These PD-1+ cells co-express granzyme B and Ki67, suggesting these are activated effector CD8+ T cells (Figure S6). Although CD8+ T cells appeared to be optimally activated in the RT tumors, there was still a significant increase in activated CD8+ T cells in the combination of mch1N11 and anti-PD-1 without RT (Figure 6C). This combination also led to significant anti-tumor activity in the absence of RT (Figures 5B and 5C). We also observed a decrease in CD4+ Foxp3+ Tregs in the tumors from the RT-treated groups. This corresponded to an increase in the CD8:Treg ratio, with the strongest effect seen in the triple-combination therapy group (Figure 6D). We found that 4PD-1^{hi} T cells are decreased after RT, with the greatest decrease observed in the triple combination (Figure 6D). In addition, the ratio of CD8 to 4PD-1^{hi} cells was significantly increased in the RT groups, with the triple combination showing the highest increase. None of the treatments had a significant effect on effector (Foxp3− PD-$1^{low/-}$) CD4+ T cell infiltration or their activation state in the tumor (data not shown).

Peripheral Blood Mononuclear Cells (PBMCs) from Melanoma Patients Demonstrated an Increase in PS Expression on Immune Subsets 4–7 Days after Tumor-Directed RT

To determine whether these preclinical findings have relevance in a clinical setting, we examined PS expression on immune subsets in the blood of melanoma patients receiving RT. Peripheral blood was collected from 7 melanoma patients before and 4–7 days after receiving tumor-directed RT to one or more metastases. Freshly isolated PBMCs from each patient were stained for PS expression using annexin V, caspase-3/7, and known lineage markers for human immune subsets on the same day the blood was collected (Figures 7A and 7B; Figure S7A). Annexin V staining of PS on viable cells was confirmed with an anti-PS antibody, which showed similar staining patterns (Figure S7B). We found that PS expression on several immune subsets increased after RT in 6 of 7 patients tested (Figure 7C). The most significant increases were seen in CD14− CD11b+ myeloid cells, $CD56^{int}$ NK cells, and CD8+ T cells, consistent with the findings in mouse studies (Figure 1E). PD-1

expression was also examined on each immune subset; however, it did not significantly change or correlate with PS expression at the time points examined, suggesting that the mechanisms and kinetics involved in regulating expression of PS are distinct from those for PD-1 (Figure S7C; data not shown). We were able to collect PBMCs before and 4 and 31 days after receiving tumor-directed RT from a single patient (Pt. 6). The increase in PS expression observed early (4 days) after RT was transient and returned to normal after 31 days (Figure S7D).

DISCUSSION

An interesting observation from this study is the finding that PS is expressed on viable immune cells in the TME. Other studies have also shown that PS is expressed on activated immune cells and the kinetics are different from apoptotic cells (Birge et al., 2016). For example, PS expression on viable cells depends on intracellular Ca^{2+}. Because the activation of T cells through TCR stimulation increases intracellular Ca^{2+}, it is not surprising that PS expression is increased on activated T cells. In addition, the density and spatial distribution of PS on the cell surface of viable and apoptotic cells may differ (Birge et al., 2016; Kumar et al., 2017). It will be interesting in the future to delineate the transcriptional and functional profile of immune cells that express PS on their surface compared with those that do not. We posit that PS acts similar to an immune checkpoint molecule on viable immune cells in which it is induced during activation and acts as a negative feedback mechanism to prevent aberrant activation of the immune system. Thus, similar to blocking immune checkpoints, blocking PS removes this feedback, allowing more potent activation of both innate and adaptive immune cells. However, removing this suppression is not sufficient to promote anti-tumor immunity, because mch1N11 as a single agent is ineffective in controlling B16 tumor growth. Additional proinflammatory signals are required to prime and boost the immune responses to the tumor. RT and PD-1 blockade can each provide these additional proinflammatory signals.

A remaining unknown is the mechanism by which PS expression is increased after RT. It appears that PS expression is highest in the tumor when inflammation in the TME is highest (10 days post-RT). This would suggest that PS expression correlates with immune cell activation. Although we observed the highest increase in PS expression on immune cells in the tumors, this effect was also seen in the spleen of treated mice and in the blood of melanoma patients receiving tumor-directed RT. This suggests a possible role for secreted or soluble factors such as cytokines. RT has also been shown to induce the secretion of multiple cytokines that recruit immune cells to the tumor site (Barker et al., 2018; Matsumura et al., 2008). Consistent with this, our results indicate that CD8+ T cells are partially responsible for the increase in PS expression on immune cells in the tumors after RT. Activated CD8+ T cells are the main producers of proinflammatory cytokines such as IFNγ in the TME and are therefore most likely responsible for the increase in PS expression in the TME. In agreement with this, we showed that cytokines such as IFNγ can increase PS expression on tumor cells *in vitro* (Figure S1D).

There is an abundance of PS receptors on the surface of immune cells. Members of the Axl/Mer/Tyro3 receptor tyrosine kinase family have been largely implicated in the clearance

of apoptotic cells expressing PS (efferocytosis). However, the specific receptor or receptors recognizing PS on viable immune cells remains unknown. The antibody used in our studies, mch1N11, does not directly bind to PS but rather binds to the adaptor protein β2-glycoprotein I (β2GPI) and blocks its interaction with PS receptors (Belzile et al., 2018). Initial studies show that β2GPI is important for the activity of PS-targeting antibodies such as mch1N11 (Ran et al., 2005). For the *in vitro* studies reported here (Figure 3C), mouse serum needed to be added to the culture to provide a source for β2GPI to efficiently block PS interaction with its receptors. The exact receptor that binds β2GPI-bound PS remains unknown. However, several receptors, including members of the Toll-like receptor (TLR) family (TLR2, TLR4, and TLR8), annexin A2, glycoprotein Ibα, and low-density lipoprotein (LDL)-receptor family-related protein (LRP) 8, also known as ApoER2, have been reported to interact with β2GPI-antibody complexes (de Groot and Urbanus, 2012). It will be interesting to decipher which PS receptor or receptors play a role in promoting an anti-inflammatory TME and which receptors are affected by mch1N11-mediated blocking of PS-β2GPI interactions.

We show that blocking PS signaling through its receptors with mch1N11 enhances local and systemic CD8+ T cell activation and, to a lesser extent, CD4+ T cell activation when combined with RT and/or PD-1 blockade (Figures 4A and 6C). In our experiments, we observed increased PS expression of adoptively transferred antigen-specific Pmel and endogenous CD8+ T cells in mice treated with RT + mch1N11 (Figure S3B). These transferred cells also show increased expression of memory and activation markers, indicating that PS expression is associated with activated effector T cells. This is consistent with previous reports that PS is externalized on the surface of activated T cells (Birge et al., 2016). In addition, the data from the experiments in Figures 4A and 6C show that the combination of mch1N11 with RT and/or anti-PD-1 enhances CD8+ T cell expression of the cytolytic protein granzyme B. We also observed enhanced CD8+ T cell-mediated killing of B16 tumor cells when mch1N11 is combined with RT and/or anti-PD-1 (Figure 6A). These data suggest that the addition of mch1N11 to RT or anti-PD-1 promotes a cytolytic program in CD8+ T cells, and this may be the main mechanism by which mch1N11 enhances the anti-tumor efficacy of RT with or without anti-PD-1. Whether blocking the PS interaction with its receptors can alter T cells directly or affect T cell activation and cytolytic programming by repolarizing the TME toward a proinflammatory environment remains an open question.

We summarized the various effects of the combination of mch1N11 with RT and anti-PD-1 on the immune system in Figure 7D. We propose that each therapy (mch1N11, RT, and anti-PD-1) has a unique mode of action and that when combined, this leads to potent activation of the immune system. In untreated animals, B16 tumors express basal levels PS on the cell surface of viable tumor and immune cells. In addition, the TAMs have an anti-inflammatory M2 phenotype and the CD8+ T cells are dysfunctional (Figure 7D, first row). Tumor-directed RT kills a fraction of tumor cells and increases PS expression on the remaining viable tumor cells and immune cells. In addition, there is a slight increase in CD8+ T cell infiltration and activation; however, the TAMs remain relatively unchanged (Figure 7D, second row). When RT is combined with mch1N11, there is an increase in CD8+ T cell infiltration and activation and proinflammatory M1 macrophages (Figure 7D, third row).

The addition of anti-PD-1 to RT and mch1N11 increases the infiltration and significantly enhances the activation state of CD8+ T cells (Figure 7D, last row). The resulting effect of the triple-combination therapy is a potent activation of both the adaptive and the innate arms of the immune system.

The therapeutic success of ICB in a subset of cancer patients has brought immunotherapy into the spotlight for further research. However, the clinical success rate of approved ICB as monotherapy remains relatively low, with 20%–40% of patients showing durable clinical responses (Zappasodi et al., 2018b). Several mechanisms of resistance have been identified that limit the efficacy ICB. Hence, there is an unmet need for new therapies to overcome these resistance mechanisms in patients. We believe that the combination of RT and PS blockade could not only make an immunologically cold tumor hot but also alleviate the suppressive mechanisms that exist in the TME. In this sense, the combination of RT and PS blockade can enhance the efficacy of ICB. The finding that melanoma patients showed an increase of PS expression on immune subsets in the blood 4–7 days after tumor-directed RT suggests that the mouse and human biology, in this respect, are similar. The clinical PS-targeting equivalent of the mouse mch1N11, bavituximab, has been used in patients and was well tolerated at doses ranging up to 3 mg/kg weekly (Gerber et al., 2011). The vast preclinical data and patient data reported here highlight the potential of using tumor-directed RT with a PS-targeting agent to enhance the clinical outcome of patients being treated with anti-PD-1. We rationalize that the patient population that would most likely benefit from novel combination therapies such as RT and PS blockade includes those who were previously treated with anti-PD-1 and did not respond or became refractory to the therapy.

STAR★METHODS

RESOURCE AVAILABILITY

Lead Contact—Further information and requests for resources and reagents should be directed to and will be fulfilled by the Lead Contact, Taha Merghoub (merghout@mskcc.org).

Materials Availability—This study did not generate new unique reagents.

Data and Code Availability

- Original/source data for [figures/datatype] in the paper are available from the corresponding authors on request.

EXPERIMENTAL MODEL AND SUBJECT DETAILS

Mouse Models—Female C57BL/6J mice (8–10 weeks) were purchased from the Jackson Laboratory (Bar Harbor, ME). Breeding pairs for Pmel-1 TCR transgenic mice (Overwijk et al., 2003) were obtained from N. Restifo (National Institutes of Health). $Sting^{Gt/Gt}$ mice in C57BL/6J background was generated in Dr. Russell Vance' s laboratory (University of California, Berkeley) (Sauer et al., 2011). We obtained breeding pairs of the C57BL/6 $Sting^{Gt/Gt}$ from Liang Deng's lab at MSK (Dai et al., 2017). For Pmel and $Sting^{Gt/Gt}$ mice, both male and female mice (8–10 weeks old) were used for experiments. Mouse experiments

were performed in accordance with institutional guidelines under a protocol approved by the Memorial Sloan Kettering Cancer Center Institutional Animal Care and Use Committee. All mice were maintained in a pathogen-free facility according to National Institutes of Health Animal Care guidelines.

Cell lines—The B16F10 mouse melanoma line was originally obtained from I. Fidler. The B16F10 Sting$^{-/-}$ cell line was generated using CRISPR/Cas9 and confirmed by western blotting. MC38 cell line was purchased from Kerafast, Inc. These cells were maintained in RPMI-1640 medium containing 7.5% fetal bovine serum (FBS) and L-glutamine. Cells were detached using 0.25% tryspin/EDTA. For cell surface staining and CD8+ T cell killing assays, cells were detached non-enzymatically using Cellstripper or 5mM EDTA.

Patient Material—All patients signed an approved informed consent before providing tissue samples. Patient samples were collected on a tissue-collection protocol approved (06–107) by the MSK Institutional Review Board. Human peripheral blood was collected from 7 patients (male and female) with metastatic cutaneous melanoma prior to and 4–7 days after receiving tumor-directed RT (27 Gy in 3 fractions of 9 Gy) to one or more sites of metastases. PBMCs were isolated from whole blood by the MSK Immune Monitoring Core Facility.

METHOD DETAILS

***In vivo* mouse experiments with tumor-directed RT and monoclonal antibody treatment—**8–10 week old C57BL/6 female mice were injected intradermally on the right hindlimb with 100,000 B16F10 cells in 50 μl (0.05mL) PBS. On day 7–10, when tumors reached ~50mm^2 in size, mice were anesthetized with isoflurane and placed in a radiation jig where only the hindlimb is exposed (Camphausen et al., 2003). The right hindlimb was irradiated with 15 Gy RT using the X-RAD 320 focus beam irradiator such that only the exposed hindlimb bearing the tumors will receive radiation. On days 1 and 4 after RT, each mouse received intraperitoneal injections (i.p.) of 0.2mg of the phosphatidylserine-targeting antibody (mch1N11) in 0.2ml of PBS. In experiments where anti-PD-1 was given, mice received 0.25mg of anti-PD-1 (clone RMP1–14) i.p. in 0.2ml of PBS on days 1, 4, and 7 after RT. For tumor measurements, each mouse was tagged by ear notching on day 5 post tumor implantation and tumor size (length and width) was measured every 3–4 days using a caliper for the duration of the experiment. Tumor measurements (surface area in mm^2) and overall survival were used to determine efficacy of the treatments.

For the bilateral tumor model, C57BL/6 mice (10 mice/group) were injected with 100,000 B16F10 melanoma cells intradermally on the right hindlimb. 5 days later, the same animals were injected with 100,000 B16F10 melanoma cells intradermally on the left flank (for abscopal tumors). On day 10 post tumor implantation, mice were treated with a single dose of 15Gy RT on the right hindlimb. On days 11 and 14, mice were injected i.p. with 200 μg/mouse of mch1N11 with or without 250 μg/mouse (given every 3 days for a total of 3 days).

CD8+ T cells were depleted by i.p. injection of 200 μg of a depleting antibody (clone 2.43) starting the same day as RT and given every 3 days thereafter until the end of the experiment.

Gene expression in *ex vivo* tumors—C57BL/6 mice (3–5 mice/group) were injected with 100,000 B16F10 melanoma cells on the right hindlimb and treated with RT and one dose of mch1N11 as described in above. Tumors were harvested 3 days after initial treatment. RNA was extracted from whole tumors and analyzed for gene expression of 43 pro- and anti- inflammatory genes that were selected based on our in-house collection of pre-optimized mouse Taqman probes (see Key Resources Table and Table S1). Tumor samples (5 mice/group) were analyzed on a 48.48 Dynamic Array integrated fluidic circuit (IFC) for Gene Expression on the Fluidigm Biomark MX/HD as per manufacturer's protocol. Gene expression data are represented as the average fold change ($2^{-\Delta\Delta CT}$) relative to the control group (Figure 3F) or normalized to GAPDH (Figure S2).

Adoptive transfer of Pmel CD8+ T cells—C57BL/6 mice (5 mice/group) were injected with 100,000 B16F10 melanoma cells on the right hindlimb. On day 10 post tumor implantation, mice were treated with a single dose of 15Gy RT on the hindlimb. Naive CD8+ T cells were purified from spleens of Pmel-1 TCR transgenic mice by magnetic-activated cell sorting (MACS) and fluorescently labeled with 1μM CFSE as previously described (Rizzuto et al., 2009). On the same day as RT (day 10), each mouse received 10^6 CFSE-labeled Pmel CD8+ T cells by tail vein injection. One day after RT (day 11), mice were injected i.p. with 200 μg/mouse of mch1N11 or isotype control. Blood, spleens, draining inguinal LNs and tumors were excised 7 days after RT (day 17) and dissociated into single cell suspensions for analysis by flow cytometry. Pmel CD8+ T cells were identified by staining for the congenic marker Thy1.1.

***In vitro* macrophage polarization—**Bone marrow (BM) from naive C57BL/6 mice were isolated and cultured in 60cm Petri dishes at 5×10^6 cells in 5 mL of complete media (RPMI with 10% fetal bovine serum (FBS) supplemented with 2mM L-glutamine, 1mM sodium pyruvate and 50 μM 2-mercaptoethanol) in the presences of 20ng/ml recombinant murine GMCSF. Cultures were fed every 2 days with fresh medium containing GMCSF. After 6 days in culture, BM cells were detached non-enzymatically using cell scrapers and re-plated in 12-well plates containing 1ml of complete medium with 5% mouse serum and 10^6 BM cells per well in the presence or absence of an isotype control (C44) or PS-targeting (mch1N11) antibody. 24 hours later, cells were detached and analyzed by flow cytometry for APCs (CD11c+, MHC II+), total macrophages (CD11b+ F4/80+), M1 (MHC II+ CD206−) and M2 (MHC II− CD206+) macrophages.

Flow Cytometry of mouse LNs, spleens, and tumors—Cells from tumor draining LNs, spleens, and tumors were prepared by mechanical dissociation in 40 μM filters and red blood cells were removed from spleens and blood using ACK lysis buffer. When tumor weight was greater than 0.1 g, cells were purified using a 40% Percoll gradient centrifugation. For staining for flow cytometry analysis: 100 μL of single cell suspensions of each tissue were plated in 96-well round bottom plates. Cells were pelleted by spinning at 2,000 rpm for 5 mins. Cells were incubated in 100 μL of 5 μg/ml Fc-block antibody (clone 2.4G2) for 20 mins on ice in FACS buffer (PBS + 0.5% BSA + 2mM EDTA). After Fc-block, cells were stained in FACS buffer containing fluorophore conjugated surface antibodies and a fixable viability dye for 20 mins on ice, then washed 2 times with 200 μL

FACS buffer. All intracellular staining was conducted using the Foxp3 fixation/permeabilization buffer according to the manufacturer's instructions. Flow cytometry was performed on a BD LSRII or Cytek Aurora. FlowJo software V10 was used for all flow cytometry analysis.

For intracellular cytokine staining, single cell suspensions of tissues were plated in 96-well round bottom plates containing 200 μL complete medium with 1 μM PMA and 1 μM Ionomycin. Plates were incubated for 30 mins at 37°C, then Brefeldin A (1:1000 dil) and 10 μg/ml Monensin was added and incubated for an additional 5 hr at 37°C. The plates were chilled at 4°C and stained for intracellular cytokine and analyzed by flow cytometry.

Annexin V and Caspase 3/7 staining of mouse tissues—C57BL/6 mice (5 mice/group) were injected with 100,000 B16F10 melanoma cells intradermally on the hindlimb, 10 days later, tumors were treated with a single dose of 15 Gy RT. Tumors were excised 1, 5 and 10 days after RT and processed for flow cytometry. 100 μL of single cell suspensions of each tissue were plated in 96-well round bottom plates. Cells were pelleted by spinning at 2,000 rpm for 5 mins. Cells were incubated in 100 μL of complete medium containing 2 μM Caspase-3/7 Green Detection Reagent and incubated at 37°C for 30 mins. Cells were chilled, pelleted and washed once with 200 μL Annexin V Binding buffer. Cells were incubated in 100 μL of 5 μg/ml Fc-block antibody (clone 2.4G2) for 20 mins on ice in Annexin V Binding buffer. Cells were pelleted then incubated at room temperature for 20 mins in the dark with 100 μL of Annexin V Binding buffer containing Annexin V-PE or anti-PS-Alexa Fluor 488 (clone 1H6), a viability dye and fluorophore conjugated cell surface antibodies. Cells were washed twice with 200 μL Annexin V Binding buffer and then analyzed by flow cytometry.

Annexin staining of melanoma patients PBMCs—Freshly isolated PBMCs from each patient were stained for PS expression using Annexin V and caspase 3/7 on the day the same day blood was collected. 1×10^6 PBMCs were plated in 96-well round bottom plates. Cells were incubated in 100 μL of complete medium containing 2 μM Caspase-3/7 Green Detection Reagent and incubated at 37°C for 30 mins. Cells were pelleted and washed once with 200 μL Annexin V Binding buffer. Cells were incubated in 50 μL of human Fc-block for 20 mins on ice in FACS buffer. Cells were pelleted then incubated on ice for 20 mins with 100 μL of FACS buffer containing fluorophore conjugated cell surface antibodies. Cells were washed twice with 200 μL Annexin V Binding buffer and the incubated in 100 μL of Annexin V Binding buffer containing Annexin V-PE or anti-PS Alexa 488 for 20 mins at room temperature in the dark. Cells were washed twice with 200 μL Annexin V Binding buffer and then analyzed by flow cytometry.

CD8+ T cell killing assay—Single cells suspensions of splenocytes were isolated from treated animals and CD8+ T cells were purified the using MACS beads according to the manufacture's protocol. 1mL complete medium containing 10^6 CD8+ T cells and 10^4 B16 tumor cells (as targets) were added to 24-well plates and incubated for 48h at 37°C. The T cells were washed away with 1mL PBS and the remining viable tumor cells were detached using 0.25% Trypsin/EDTA. The detached tumor cells were diluted and plated in six-well plates for colony formation. Seven days later, plates were fixed with 3.7% formaldehyde and

stained with 2% methylene blue as previously described (Budhu et al., 2010). Colonies were counted manually to assess number of viable cells.

QUANTIFICATION AND STATISTICAL ANALYSIS

Unless otherwise indicated p values were calculated using a 2-tailed Student's t test or two-way ANOVA-test corrected for multiple comparisons. A p value of < 0.05 was considered statistically significant. Overall survival curves and median survival (days) of each treatment group was obtained from pooled replicate experiments and analyzed using Kaplan–Meier estimator. The survival curves measure time from start of experiment to tumor diameter of 2cm (in which case the mouse needs to be euthanized) or death. However, the tumor volume curves averaged at each time point per group are only reported for as long as all mice in a group are alive. p values comparing survival curves were calculated using the Log-rank (Mantel-Cox) test. Correlations of T cell frequencies with tumor weight were done using Pearson's correlation.

All graphs and statistical calculations were done using GraphPad Prism software and Microsoft Excel.

Supplementary Material

Refer to Web version on PubMed Central for supplementary material.

ACKNOWLEDGMENTS

This research was funded partly through NIH/NCI Cancer Center support grant P30 CA008748, NIH/NCI R01 CA056821, the Swim Across America, Ludwig Institute for Cancer Research, Ludwig Center for Cancer Immunotherapy at Memorial Sloan Kettering, Cancer Research Institute, Parker Institute for Cancer Immunotherapy, and Breast Cancer Research Foundation. R.G. received support from an NIH NCI-T32 postdoctoral research fellowship. A.G. received support from the Howard Hughes Medical Institute's Medical Research Fellows Program. R.Z. received support from the Parker Bridge Scholar Award. We thank the Immune Monitoring Core Facility at the Memorial Sloan Kettering Cancer Center for technical assistance.

DECLARATION OF INTERESTS

All authors concur with the submission of this manuscript and have no financial or other interests related to the submitted work. T.M. is a cofounder and holds an equity in IMVAQ Therapeutics. He is a consultant of Immunos Therapeutics and Pfizer. He has research support from Bristol Myers Squibb; Surface Oncology; Kyn Therapeutics; Infinity Pharmaceuticals, Inc.; Peregrine Pharmaceuticals, Inc.; Adaptive Biotechnologies; Leap Therapeutics, Inc.; and Aprea. He has patents on applications related to work on oncolytic viral therapy, alpha virus-based vaccine, neoantigen modeling, CD40, GITR, OX40, PD-1, and CTLA-4. J.D.W. is a consultant for Adaptive Biotech, Advaxis, Amgen, Apricity, Array BioPharma, Ascentage Pharma, Astellas, Bayer, Beigene, Bristol Myers Squibb, Celgene, Chugai, Elucida, Eli Lilly, F Star, Genentech, Imvaq, Janssen, Kleo Pharma, Linnaeus, MedImmune, Merck, Neon Therapeutics, Ono, Polaris Pharma, Polynoma, Psioxus, Puretech, Recepta, Trieza, Sellas Life Sciences, Serametrix, Surface Oncology, and Syndax. Research support: Bristol Myers Squibb, Medimmune, Merck Pharmaceuticals, and Genentech. Equity: Potenza Therapeutics, Tizona Pharmaceuticals, Adaptive Biotechnologies, Elucida, Imvaq, Beigene, Trieza, and Linnaeus. Honorarium: Esanex. Patents: xenogeneic DNA vaccines, alphavirus replicon particles expressing TRP2, MDSC assay, Newcastle disease viruses for cancer therapy, genomic signature to identify responders to ipilimumab in melanoma, engineered vaccinia viruses for cancer immunotherapy, anti-CD40 agonist monoclonal antibody (mAb) fused to monophosphoryl lipid A (MPL) for cancer therapy, CAR+ T cells targeting differentiation antigens as means to treat cancer, anti-PD-1 antibody, anti-CTLA-4 antibodies, and anti-GITR antibodies and methods of use thereof. L.D. is a cofounder and holds equity in IMVAQ Therapeutics. She has patents on applications related to work on oncolytic viral therapy. R.Z. is inventor on patent applications related to work on GITR, PD-1, and CTLA-4. R.Z. is consultant for Leap Therapeutics and iTEOS Belgium SA. C.A.B. is a consultant of Regeneron. He has research support from Amgen and Merck.

REFERENCES

Apetoh L, Ghiringhelli F, Tesniere A, Obeid M, Ortiz C, Criollo A, Mignot G, Maiuri MC, Ullrich E, Saulnier P, et al. (2007). Toll-like receptor 4-dependent contribution of the immune system to anticancer chemotherapy and radiotherapy. Nat. Med 13, 1050–1059. [PubMed: 17704786]

Barker CA, Kim SK, Budhu S, Matsoukas K, Daniyan AF, and D'Angelo SP (2018). Cytokine release syndrome after radiation therapy: case report and review of the literature. J. Immunother. Cancer 6, 1. [PubMed: 29298730]

Belzile O, Huang X, Gong J, Carlson J, Schroit AJ, Brekken RA, and Freimark BD (2018). Antibody targeting of phosphatidylserine for the detection and immunotherapy of cancer. ImmunoTargets Ther 7, 1–14. [PubMed: 29417044]

Birge RB, Boeltz S, Kumar S, Carlson J, Wanderley J, Calianese D, Barcinski M, Brekken RA, Huang X, Hutchins JT, et al. (2016). Phosphatidylserine is a global immunosuppressive signal in efferocytosis, infectious disease, and cancer. Cell Death Differ 23, 962–978. [PubMed: 26915293]

Budhu S, Loike JD, Pandolfi A, Han S, Catalano G, Constantinescu A, Clynes R, and Silverstein SC (2010). CD8+ T cell concentration determines their efficiency in killing cognate antigen-expressing syngeneic mammalian cells *in vitro* and in mouse tissues. J. Exp. Med 207, 223–235. [PubMed: 20065066]

Camphausen K, Moses MA, Ménard C, Sproull M, Beecken WD, Folkman J, and O'Reilly MS (2003). Radiation abscopal antitumor effect is mediated through p53. Cancer Res 63, 1990–1993. [PubMed: 12702593]

Chen HY, Xu L, Li LF, Liu XX, Gao JX, and Bai YR (2018). Inhibiting the $CD8^+$ T cell infiltration in the tumor microenvironment after radiotherapy is an important mechanism of radioresistance. Sci. Rep 8, 11934. [PubMed: 30093664]

Dai P, Wang W, Yang N, Serna-Tamayo C, Ricca JM, Zamarin D, Shuman S, Merghoub T, Wolchok JD, and Deng L (2017). Intratumoral delivery of inactivated modified vaccinia virus Ankara (iMVA) induces systemic antitumor immunity via STING and Batf3-dependent dendritic cells. Sci. Immunol 2, eaal1713. [PubMed: 28763795]

de Groot PG, and Urbanus RT (2012). The significance of autoantibodies against β2-glycoprotein I. Blood 120, 266–274. [PubMed: 22553312]

Deng L, Liang H, Burnette B, Beckett M, Darga T, Weichselbaum RR, and Fu YX (2014). Irradiation and anti-PD-L1 treatment synergistically promote antitumor immunity in mice. J. Clin. Invest 124, 687–695. [PubMed: 24382348]

Diamond JM, Vanpouille-Box C, Spada S, Rudqvist NP, Chapman JR, Ueberheide BM, Pilones KA, Sarfraz Y, Formenti SC, and Demaria S (2018). Exosomes Shuttle TREX1-Sensitive IFN-Stimulatory dsDNA from Irradiated Cancer Cells to DCs. Cancer Immunol. Res 6, 910–920. [PubMed: 29907693]

Formenti SC, Rudqvist NP, Golden E, Cooper B, Wennerberg E, Lhuillier C, Vanpouille-Box C, Friedman K, Ferrari de Andrade L, Wucherpfennig KW, et al. (2018). Radiotherapy induces responses of lung cancer to CTLA-4 blockade. Nat. Med 24, 1845–1851. [PubMed: 30397353]

Freimark BD, Gong J, Ye D, Gray MJ, Nguyen V, Yin S, Hatch MM, Hughes CC, Schroit AJ, Hutchins JT, et al. (2016). Antibody-Mediated Phosphatidylserine Blockade Enhances the Antitumor Responses to CTLA-4 and PD-1 Antibodies in Melanoma. Cancer Immunol. Res 4, 531–540. [PubMed: 27045021]

Gameiro SR, Jammeh ML, Wattenberg MM, Tsang KY, Ferrone S, and Hodge JW (2014). Radiation-induced immunogenic modulation of tumor enhances antigen processing and calreticulin exposure, resulting in enhanced T-cell killing. Oncotarget 5, 403–416. [PubMed: 24480782]

Gerber DE, Stopeck AT, Wong L, Rosen LS, Thorpe PE, Shan JS, and Ibrahim NK (2011). Phase I safety and pharmacokinetic study of bavituximab, a chimeric phosphatidylserine-targeting monoclonal antibody, in patients with advanced solid tumors. Clin. Cancer Res 17, 6888–6896. [PubMed: 21989064]

Golden EB, Demaria S, Schiff PB, Chachoua A, and Formenti SC (2013). An abscopal response to radiation and ipilimumab in a patient with metastatic non-small cell lung cancer. Cancer Immunol. Res 1, 365–372. [PubMed: 24563870]

Graham DK, DeRyckere D, Davies KD, and Earp HS (2014). The TAM family: phosphatidylserine sensing receptor tyrosine kinases gone awry in cancer. Nat. Rev. Cancer 14, 769–785. [PubMed: 25568918]

Gray MJ, Gong J, Hatch MM, Nguyen V, Hughes CC, Hutchins JT, and Freimark BD (2016). Phosphatidylserine-targeting antibodies augment the anti-tumorigenic activity of anti-PD-1 therapy by enhancing immune activation and downregulating pro-oncogenic factors induced by T-cell checkpoint inhibition in murine triple-negative breast cancers. Breast Cancer Res 18, 50. [PubMed: 27169467]

Gupta A, Probst HC, Vuong V, Landshammer A, Muth S, Yagita H, Schwendener R, Pruschy M, Knuth A, and van den Broek M (2012). Radiotherapy promotes tumor-specific effector CD8+ T cells via dendritic cell activation. J. Immunol 189, 558–566. [PubMed: 22685313]

He J, Yin Y, Luster TA, Watkins L, and Thorpe PE (2009). Antiphosphatidylserine antibody combined with irradiation damages tumor blood vessels and induces tumor immunity in a rat model of glioblastoma. Clin. Cancer Res 15, 6871–6880. [PubMed: 19887482]

Hiniker SM, Chen DS, Reddy S, Chang DT, Jones JC, Mollick JA, Swetter SM, and Knox SJ (2012). A systemic complete response of metastatic melanoma to local radiation and immunotherapy. Transl. Oncol 5, 404–407. [PubMed: 23323154]

Huang X, Bennett M, and Thorpe PE (2005). A monoclonal antibody that binds anionic phospholipids on tumor blood vessels enhances the antitumor effect of docetaxel on human breast tumors in mice. Cancer Res 65, 4408–4416. [PubMed: 15899833]

Kumar S, Calianese D, and Birge RB (2017). Efferocytosis of dying cells differentially modulate immunological outcomes in tumor microenvironment. Immunol. Rev 280, 149–164. [PubMed: 29027226]

Lee Y, Auh SL, Wang Y, Burnette B, Wang Y, Meng Y, Beckett M, Sharma R, Chin R, Tu T, et al. (2009). Therapeutic effects of ablative radiation on local tumor require CD8+ T cells: changing strategies for cancer treatment. Blood 114, 589–595. [PubMed: 19349616]

Lugade AA, Moran JP, Gerber SA, Rose RC, Frelinger JG, and Lord EM (2005). Local radiation therapy of B16 melanoma tumors increases the generation of tumor antigen-specific effector cells that traffic to the tumor. J. Immunol 174, 7516–7523. [PubMed: 15944250]

Matsumura S, Wang B, Kawashima N, Braunstein S, Badura M, Cameron TO, Babb JS, Schneider RJ, Formenti SC, Dustin ML, and Demaria S (2008). Radiation-induced CXCL16 release by breast cancer cells attracts effector T cells. J. Immunol. 181, 3099–3107. [PubMed: 18713980]

Mineo C, Lanier L, Jung E, Sengupta S, Ulrich V, Sacharidou A, Tarango C, Osunbunmi O, Shen YM, Salmon JE, et al. (2016). Identification of a Monoclonal Antibody That Attenuates Antiphospholipid Syndrome-Related Pregnancy Complications and Thrombosis. PLoS ONE 11, e0158757. [PubMed: 27463336]

Okwan-Duodu D, Pollack BP, Lawson D, and Khan MK (2015). Role of radiation therapy as immune activator in the era of modern immunotherapy for metastatic malignant melanoma. Am. J. Clin. Oncol 38, 119–125. [PubMed: 23648438]

Overwijk WW, Theoret MR, Finkelstein SE, Surman DR, de Jong LA, Vyth-Dreese FA, Dellemijn TA, Antony PA, Spiess PJ, Palmer DC, et al. (2003). Tumor regression and autoimmunity after reversal of a functionally tolerant state of self-reactive CD8+ T cells. J. Exp. Med 198, 569–580. [PubMed: 12925674]

Panaretakis T, Kepp O, Brockmeier U, Tesniere A, Bjorklund AC, Chapman DC, Durchschlag M, Joza N, Pierron G, van Endert P, et al. (2009). Mechanisms of pre-apoptotic calreticulin exposure in immunogenic cell death. EMBO J 28, 578–590. [PubMed: 19165151]

Postow MA, Callahan MK, Barker CA, Yamada Y, Yuan J, Kitano S, Mu Z, Rasalan T, Adamow M, Ritter E, et al. (2012). Immunologic correlates of the abscopal effect in a patient with melanoma. N. Engl. J. Med 366, 925–931. [PubMed: 22397654]

Ran S, He J, Huang X, Soares M, Scothorn D, and Thorpe PE (2005). Antitumor effects of a monoclonal antibody that binds anionic phospholipids on the surface of tumor blood vessels in mice. Clin. Cancer Res 11, 1551–1562. [PubMed: 15746060]

Rizzuto GA, Merghoub T, Hirschhorn-Cymerman D, Liu C, Lesokhin AM, Sahawneh D, Zhong H, Panageas KS, Perales MA, Altan-Bonnet G, et al. (2009). Self-antigen-specific CD8+ T cell

precursor frequency determines the quality of the antitumor immune response. J. Exp. Med 206, 849–866. [PubMed: 19332877]

Rodriguez-Ruiz ME, Rodriguez I, Garasa S, Barbes B, Solorzano JL, Perez-Gracia JL, Labiano S, Sanmamed MF, Azpilikueta A, Bolaños E, et al. (2016). Abscopal Effects of Radiotherapy Are Enhanced by Combined Immunostimulatory mAbs and Are Dependent on CD8 T Cells and Crosspriming. Cancer Res 76, 5994–6005. [PubMed: 27550452]

Sauer JD, Sotelo-Troha K, von Moltke J, Monroe KM, Rae CS, Brubaker SW, Hyodo M, Hayakawa Y, Woodward JJ, Portnoy DA, and Vance RE (2011). The N-ethyl-N-nitrosourea-induced Goldenticket mouse mutant reveals an essential function of Sting in the *in vivo* interferon response to Listeria monocytogenes and cyclic dinucleotides. Infect. Immun 79, 688–694. [PubMed: 21098106]

Sharma B, and Kanwar SS (2018). Phosphatidylserine: A cancer cell targeting biomarker. Semin. Cancer Biol 52, 17–25. [PubMed: 28870843]

Siva S, MacManus MP, Martin RF, and Martin OA (2015). Abscopal effects of radiation therapy: a clinical review for the radiobiologist. Cancer Lett 356, 82–90. [PubMed: 24125863]

Stamell EF, Wolchok JD, Gnjatic S, Lee NY, and Brownell I (2013). The abscopal effect associated with a systemic anti-melanoma immune response. Int. J. Radiat. Oncol. Biol. Phys 85, 293–295. [PubMed: 22560555]

Twyman-Saint Victor C, Rech AJ, Maity A, Rengan R, Pauken KE, Stelekati E, Benci JL, Xu B, Dada H, Odorizzi PM, et al. (2015). Radiation and dual checkpoint blockade activate non-redundant immune mechanisms in cancer. Nature 520, 373–377. [PubMed: 25754329]

Vanpouille-Box C, Alard A, Aryankalayil MJ, Sarfraz Y, Diamond JM, Schneider RJ, Inghirami G, Coleman CN, Formenti SC, and Demaria S (2017). DNA exonuclease Trex1 regulates radiotherapy-induced tumour immunogenicity. Nat. Commun 8, 15618. [PubMed: 28598415]

Yin Y, Huang X, Lynn KD, and Thorpe PE (2013). Phosphatidylserine-targeting antibody induces M1 macrophage polarization and promotes myeloid-derived suppressor cell differentiation. Cancer Immunol. Res 1, 256–268. [PubMed: 24777853]

Zappasodi R, Budhu S, Hellmann MD, Postow MA, Senbabaoglu Y, Manne S, Gasmi B, Liu C, Zhong H, Li Y, et al. (2018a). Non-conventional Inhibitory $CD4^{+}Foxp3^{-}PD\text{-}1^{hi}$ T Cells as a Biomarker of Immune Checkpoint Blockade Activity. Cancer Cell 33, 1017–1032.e7. [PubMed: 29894689]

Zappasodi R, Merghoub T, and Wolchok JD (2018b). Emerging Concepts for Immune Checkpoint Blockade-Based Combination Therapies. Cancer Cell 34, 690. [PubMed: 30300584]

Highlights

- PS expression on immune cells in murine melanoma is increased after tumor-directed RT
- Blocking PS interaction with its receptors enhances the anti-tumor efficacy of RT
- PD-1 blockade further potentiates the anti-tumor responses
- Melanoma patients' PBMCs exhibit an increase in PS expression after RT

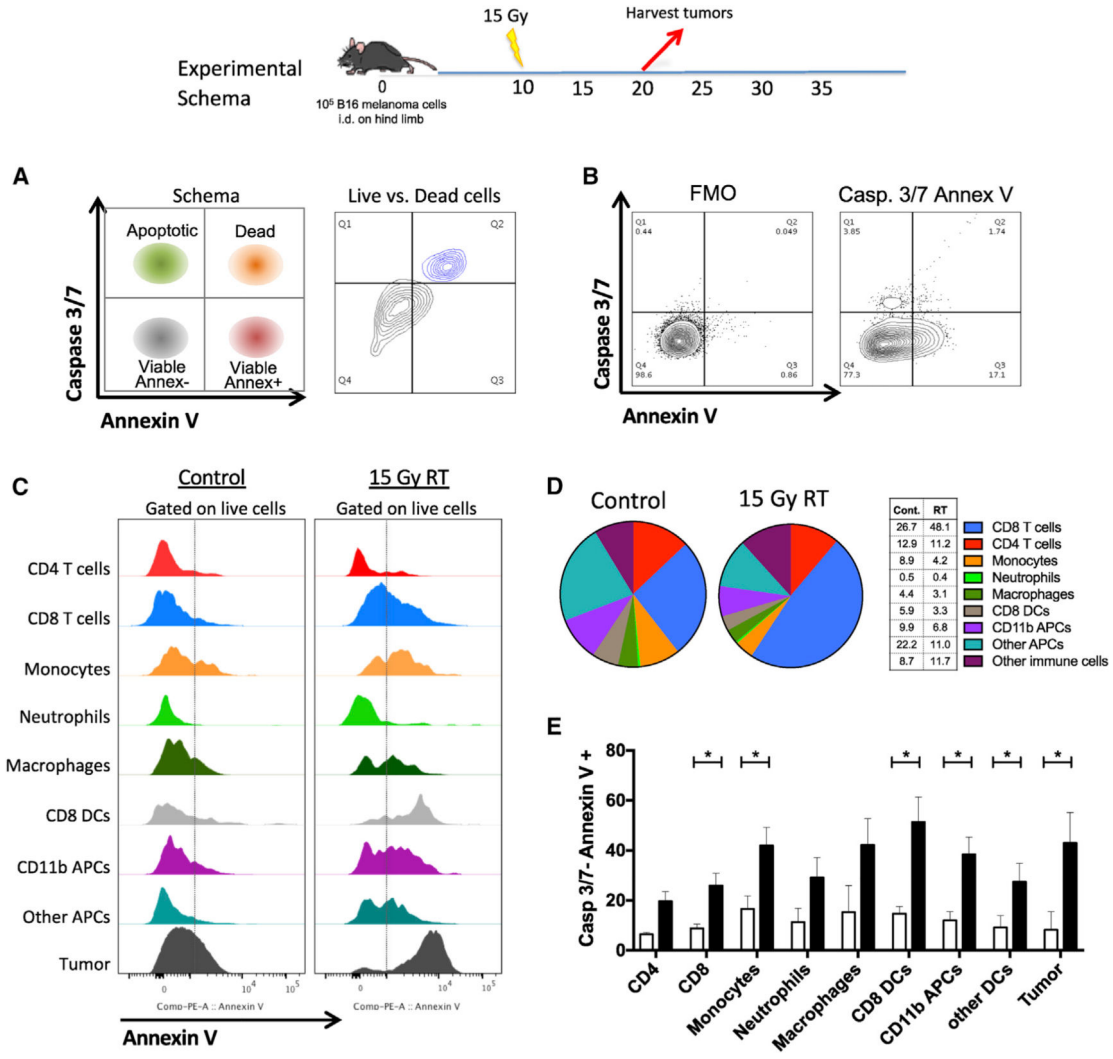

Figure 1. PS Expression on Immune Subsets in the Tumor Increases after RT

C57BL/6 mice were injected with 100,000 B16F10 melanoma cells intradermally on the hindlimb. 10 days later, tumor-bearing hindlimbs received 15 Gy RT. 10 days thereafter, tumors were excised and analyzed by flow cytometry.

(A) Schema and representative plots showing caspase-3/7 activity and PS expression on live (blue) versus dead (gray) tumor cells determined by a viability dye.

(B) Representative gating strategy used to measure PS expression using viable CD8+ T cells from the tumor as an example. Gating was based on caspase-3/7 and annexin V fluorescence minus one (FMO).

(C) Relative expression of PS on viable immune cell subsets in the tumors of mice with and without tumor-directed RT.

(D) Frequencies of immune cells as a percentage of live CD45+ cells in the tumor with and without tumor-directed RT. The tables next to the figure legend lists the percentages shown in the pie charts.

(E) Quantification of annexin V+ immune and tumor cells ±SEM (3–5 mice per group) from control tumors (white bars) and RT tumors (black bars). *p < 0.05.

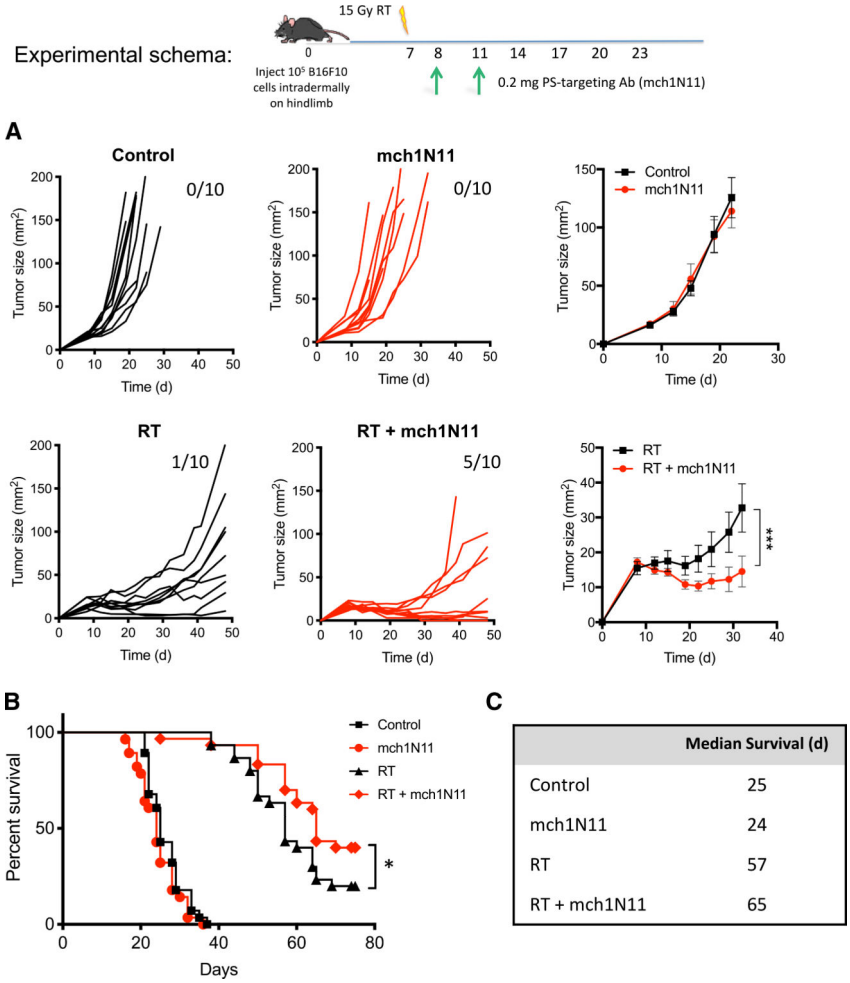

Figure 2. Targeting PS in Combination with Radiation Promotes Anti-tumor Activity in B16 Melanoma

C57BL/6 mice were injected with 100,000 B16F10 melanoma cells intradermally on the right hindlimb. 7 days post-implantation, mice were treated with a single dose of 15 Gy RT on the right hindlimb. On days 8 and 11, mice were injected i.p. with 200 μg/mouse of mch1N11 or isotype control.

(A) Individual tumor growth curves and average tumor surface area (in square millimeters) from a representative experiment. Inset numbers indicate the number of mice that completely regressed their tumors. ***$p < 0.005$.

(B and C) Overall survival (B) and median survival (C) (in days) for each treatment group pooled from 3 experiments containing 28–30 mice per group. *$p < 0.05$. The p values were calculated using a log rank (Mantel-Cox) test.

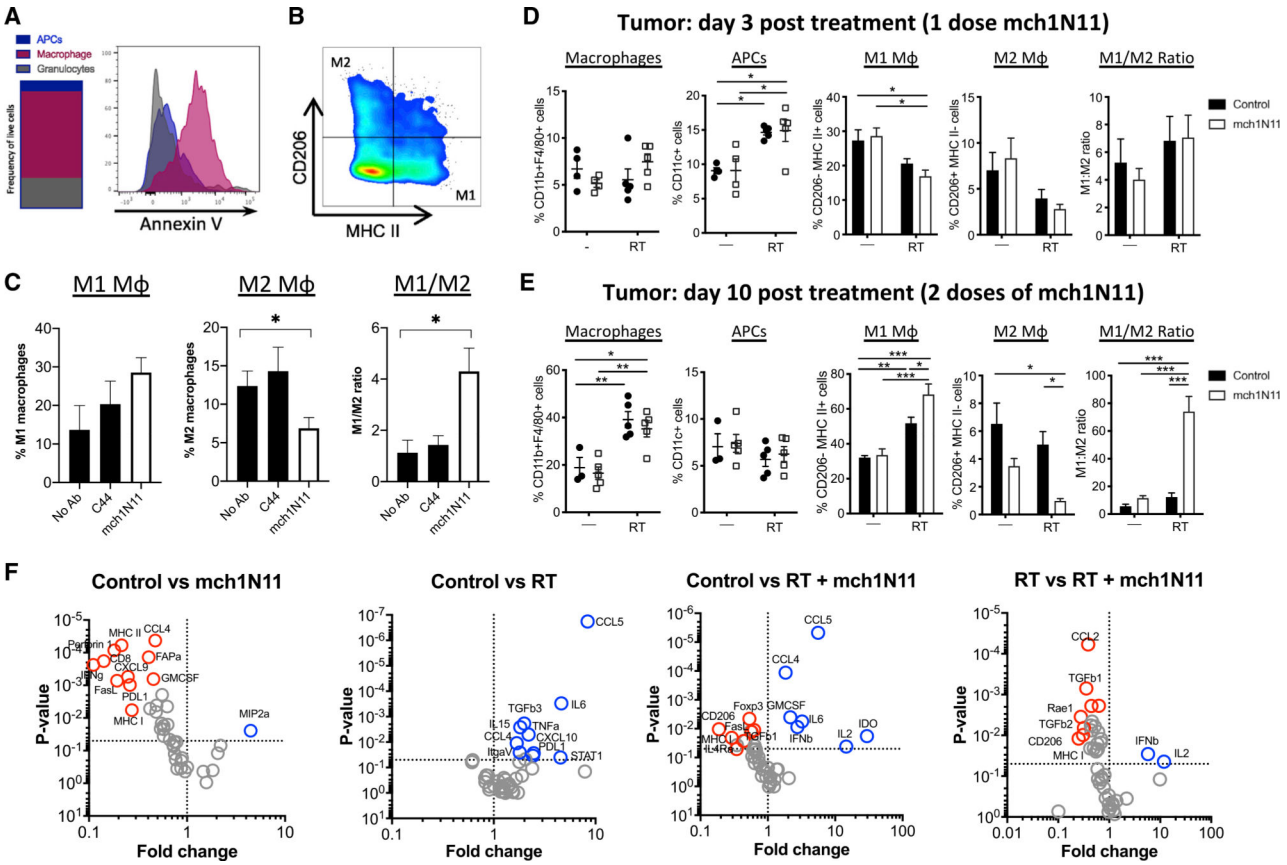

Figure 3. Targeting PS with mch1N11 Promotes a Proinflammatory TME

(A–C) Bone marrow (BM) from naive C57BL/6 mice was isolated and cultured in the presence of 20 ng/mL of granulocyte-macrophage colony-stimulating factor (GM-CSF). 6 days after culture, BM cells were isolated and replated in 12-well plates in the presence or absence of a control isotype (C44) or PS-targeting antibody (mch1N11). 24 h later, cells were detached and analyzed by flow cytometry for APCs (CD11c+ MHC II+), total macrophages (CD11b+ F4/80+), M1 macrophages (MHC II+ CD206−), and M2 macrophages (MHC II− CD206+). (A) Left: abundance of macrophages, APCs, and granulocytes in the BM cultures after 6 days. Right: expression of PS on the surface of each cell type as measured by annexin V staining on live cells. (B) Gating strategy used to identify M1 and M2 macrophages. (C) Quantification of M1 and M2 macrophages ± SEM pooled from 3 experiments.

(D–E) C57BL/6 mice were injected with B16F10 melanoma cells and treated according to the experiment outlined in Figures 2 and here. 10 days after the initial treatment, tumors were isolated from each treatment group and analyzed by flow cytometry. With 3–5 mice per group, statistics were calculated using two-way ANOVA corrected for multiple comparisons. *$p < 0.05$, **$p < 0.01$, ***$p < 0.005$.

(F) Tumors were harvested 3 days after initial treatment. RNA was extracted from whole tumors and analyzed for expression of 43 preselected genes (Table S1) using the Fluidigm Biomark MX/HD system, as described in STAR Methods. Gene expression data are represented as the average fold change ($2^{-\Delta\Delta CT}$) relative to the control group versus the

calculated p values to represent significant increase (>1 fold change and $p > 0.05$, blue circles) and decrease (<1 fold change and $p > 0.05$, red circles) in gene expression.

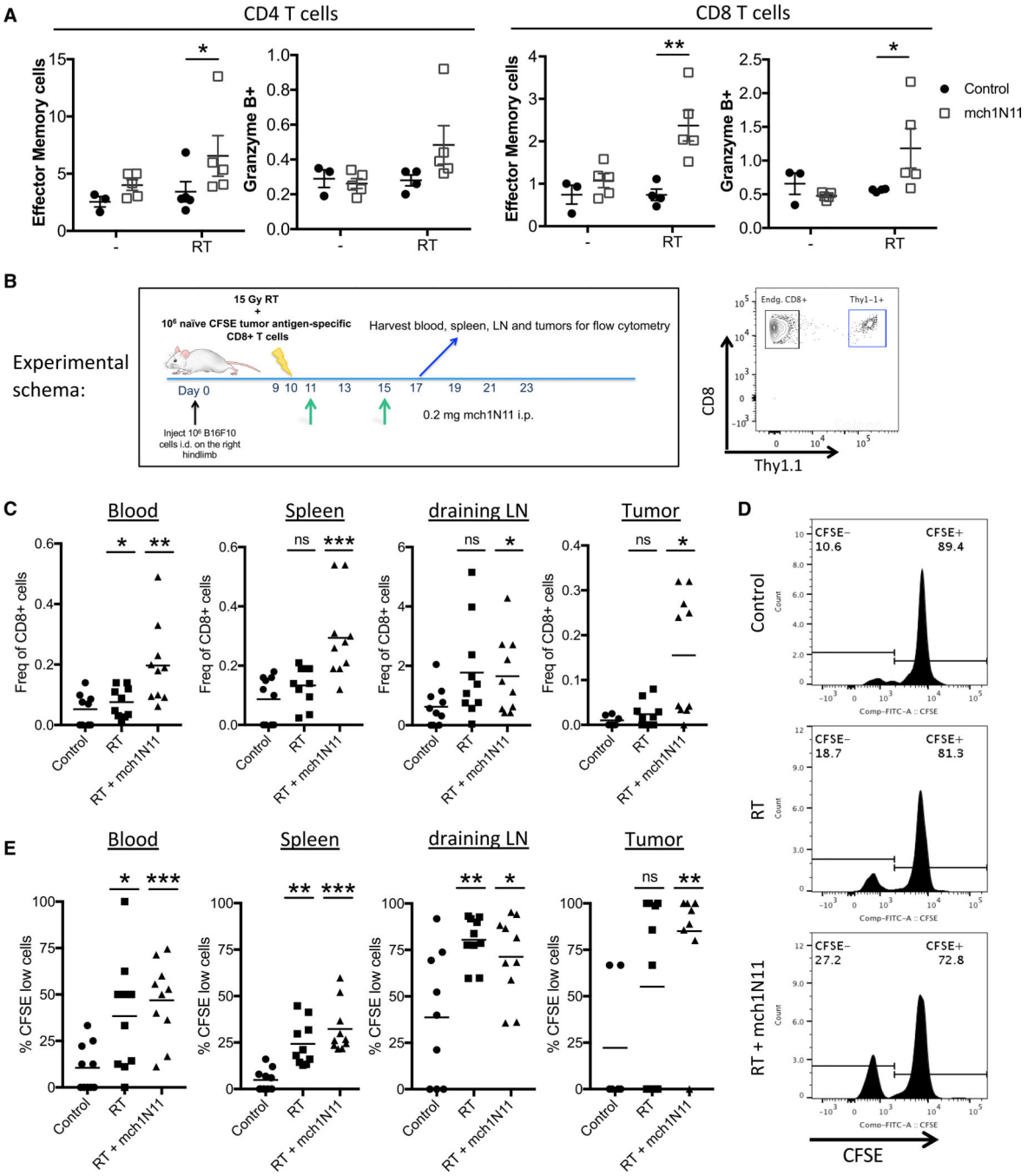

Figure 4. Targeting PS Enhances Antigen-Specific T Cell Priming in Response to RT

(A) C57BL/6 mice were injected with B16F10 melanoma cells and treated according to the experiment schema in Figure 2. 10 days after the initial treatment, tumor-draining LNs were isolated and analyzed by flow cytometry. Plotted are the frequencies of effector memory (CD44+ CD62L−) and granzyme B+ cells as a percentage of the total CD4+ and CD8+ T cell populations ±SEM (3–5 mice/group).

(B) C57BL/6 mice were injected with B16F10 melanoma cells on the right hindlimb. 10 days post-implantation, mice received 15 Gy RT locally and 10^6 naive Pmel CD8+ T cells

labeled with 1 μM CFSE by tail vein injection. On day 11, mice were injected i.p. with mch1N11 or isotype control. On day 17, blood, spleen, tumor-draining LNs, and tumors were excised and analyzed by flow cytometry. Right: representative plot of CD8+ cells versus Thy1.1 to identify the Pmel T cells.

(C) Frequencies of the Pmel CD8 T cells in the different tissues relative to the total CD8+ population.

(D) Representative plots of CFSE-labeled Pmel CD8+ T cells in the spleen to examine their proliferation ($CFSE^{low/-}$).

(E) Frequencies of proliferated Pmel CD8+ T cells in the different tissues. 6–10 mice per group. ns, not significant; *$p < 0.05$, **$p < 0.01$, ***$p < 0.005$.

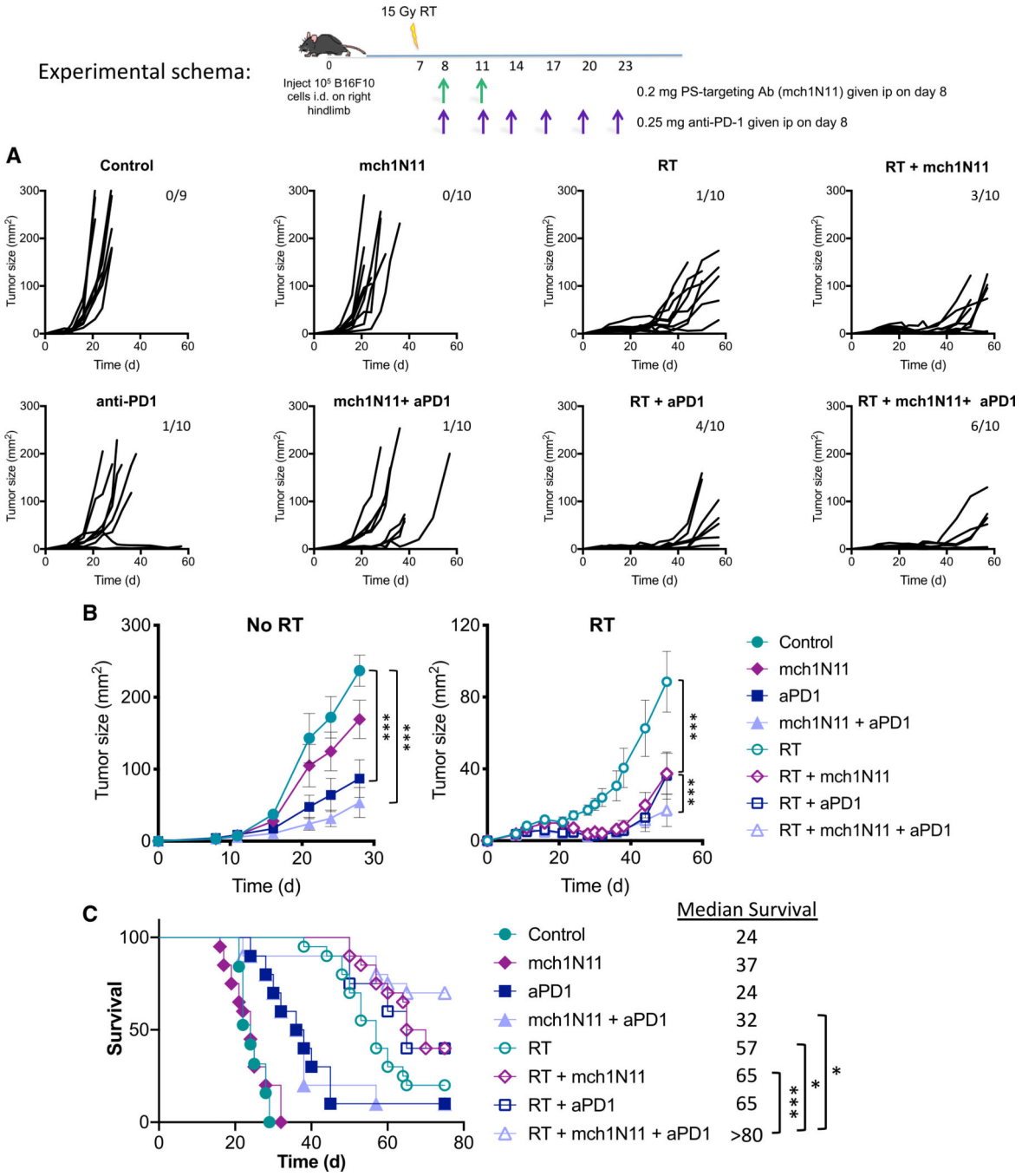

Figure 5. Targeting PS Enhances the Anti-tumor Activity of Radiation and Anti-PD-1 in B16 Melanoma

C57BL/6 mice were injected with 100,000 B16F10 melanoma cells intradermally on the right hindlimb and treated as outlined in the experimental schema.

(A) Individual tumor growth curves (in square millimeters) of a representative experiment. Inset numbers indicate the number of mice that completely regressed their tumors.

(B) Average tumor size (in square millimeters). The p values for tumor growth curves were calculated using t tests corrected for multiple comparisons (Bonferroni-Dunn).

(C) Overall survival and median survival (in days) of each treatment group from pooled experiments (n = 3). The p values were calculated using a log rank (Mantel-Cox) test. *p < 0.05, **p < 0.01, ***p < 0.005.

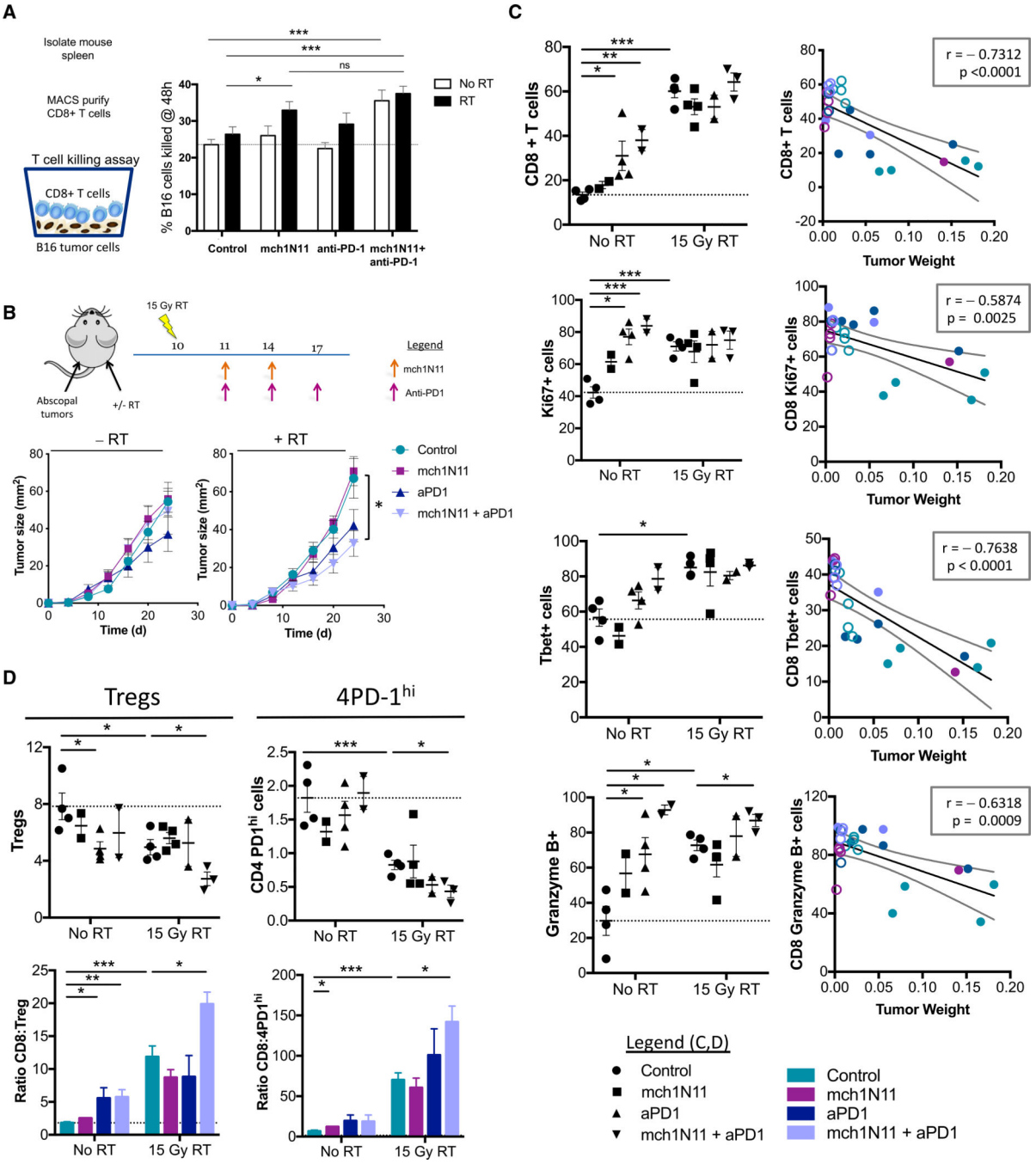

Figure 6. Targeting PS in Combination with Radiation Therapy and Anti-PD-1 Promotes CD8+ T Cell Activation in the Tumor

(A) C57BL/6 mice were injected with B16F10 cells and treated according to the experiment schema outlined in Figure 5. 10 days after RT, 10^6 CD8+ T cells purified from spleens of treated animals were co-cultured with 10^4 B16 tumor cells as targets for 48 h in 24-well plates for a T cell killing assay as previously described (Budhu et al., 2010). Shown are the average percentage ± SEM of B16 cells killed from 5 mice/group.

(B) C57BL/6 mice were injected with B16F10 cells on the right hindlimb on day 0 and left flank on day 5 and treated with RT on day 10, as outlined in the schema and described in

STAR Methods. Shown are average tumor size (in square millimeters) ± SEM of abscopal tumors only (10 mice/group). Statistics were calculated at day 25 post-tumor implantation. (C and D) C57BL/6 mice were injected with B16F10 cells and treated according to the experiment schema outlined in Figure 5. 10 days after the initial treatment, tumors were isolated from each treatment group, weighed, and analyzed by flow cytometry. (C) CD8+ T cell infiltration and activation. Left: frequencies of CD8+ T cells in tumors and their activation markers. Right: correlation between frequencies and tumor weight (in grams); closed circles represent no RT, and open circles represent RT groups. (D) Frequencies of CD4+ Foxp3+ Tregs and CD4+ Foxp3− PD-1^{hi} T cells (CD4+ PD-1^{hi} or 4PD-1^{hi}) infiltrating tumors and the ratio of CD8 to Tregs or 4PD-1^{hi}. *$p < 0.05$, **$p < 0.01$, ***$p < 0.005$.

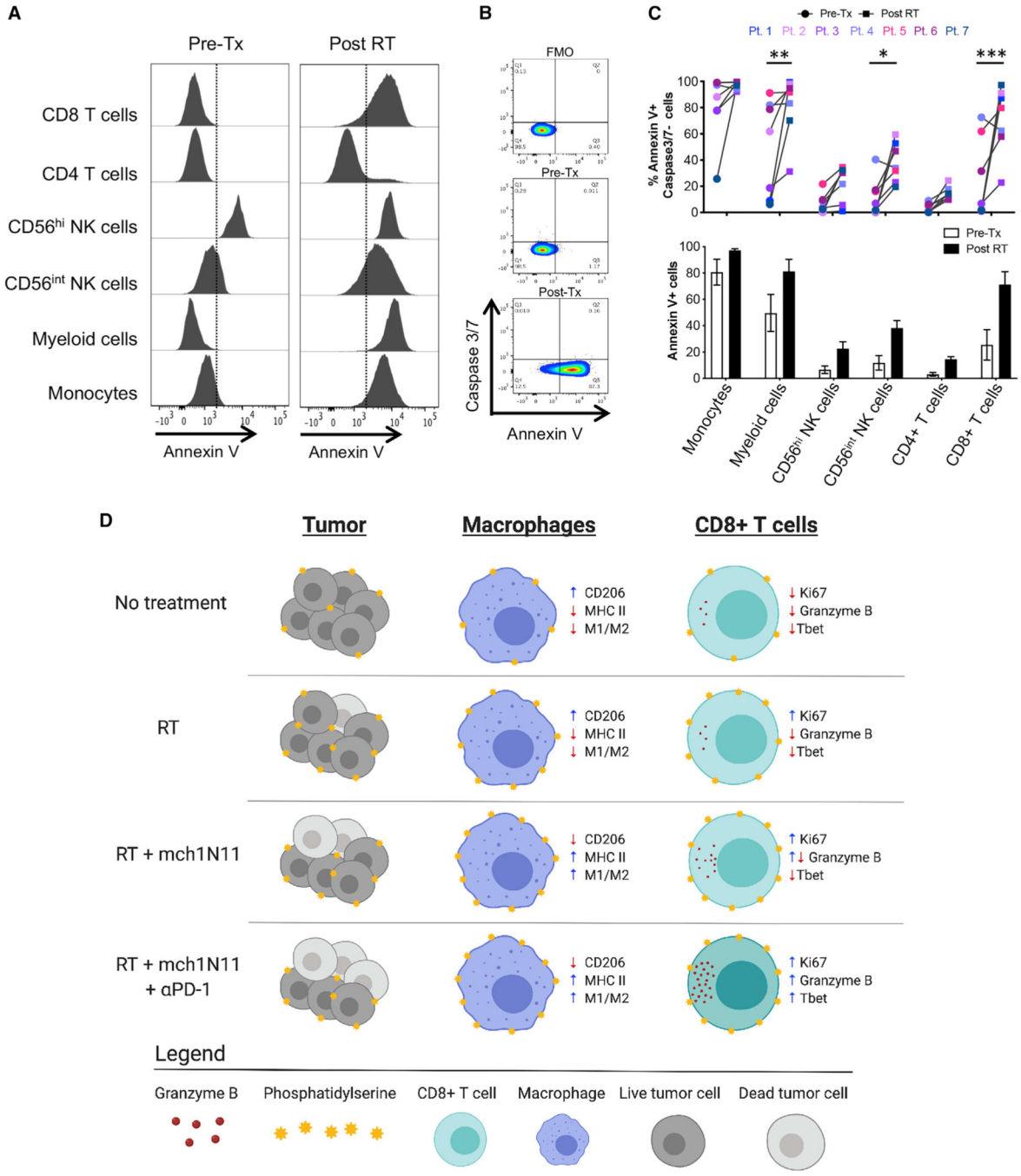

Figure 7. Melanoma Patients Demonstrated an Overall Increase of PS Expression on Immune Subsets in the Blood 4–7 Days after RT

Peripheral blood was collected from 7 melanoma patients before and 4–7 days after receiving tumor-directed RT. Freshly isolated PBMCs from each patient were stained for PS expression using annexin V on the day the blood was collected, as described in STAR Methods.

(A) Histogram plots of annexin V staining of viable immune cell subsets in PBMCs from a single patient (Pt. 1) pretreatment (Tx) and post-RT.

(B) Representative plots gated on live CD3+ CD8+ T cells of annexin V versus caspase-3/7 activity of PBMCs from a single patient pre-RT and 4 days post-RT. FMO, control.
(C) Top: individual values for each patient. Bottom: average percentage ± SEM of annexin V + immune cell subsets pre-RT and post-RT. *$p < 0.05$, ***$p < 0.005$.
(D) Model summarizing the effects of targeting PS with RT and anti-PD-1 on immune cell activation.

KEY RESOURCES TABLE

REAGENT or RESOURCE	SOURCE	IDENTIFIER
Antibodies		
Mouse mch1N11 (PS targeting antibody)	Oncologie	N/A
Mouse isotype control (clone C44)	Oncologie	N/A
Mouse anti-PD1 (clone RMP1-14)	Bioxcell	Cat# BE0146, RRID:AB_10949053
Mouse anti-CD8 (clone 2.43)	Bioxcell	Cat# BE0061, RRID:AB_1125541
Mouse CD8a MicroBeads	Miltenyi Biotech	Cat# 130-117-044
mouse Fc-block (clone 2.4G2)	MSKCC Antibody core	N/A
human Fc-block	Miltenyi Biotech	Cat# 130-059-901
anti-PS, Alexa Flour 488 (clone 1H6)	Millipore - Sigma	Cat# 16-256, RRID:AB_492616
Anti-CD8 PE-Texas Red	ThermoFisher Scientific	Cat# MCD0817, RRID:AB_1488461
Anti-CD8 PE-Cy7	BD Biosciences	Cat# 557654, RRID:AB_396769
Anti-CD8 PE	BD Biosciences	Cat# 553033, RRID:AB_394571
Anti-Ly6G Percp-Cy5.5	BD Biosciences	Cat# 560602, RRID:AB_1727563
Anti-Ly6C PE-Cy7	BD Biosciences	Cat# 560593, RRID:AB_1727557
Anti-CD4 V450	BD Biosciences	Cat# 560468, RRID:AB_1645271
Anti-CD11c APC	BD Biosciences	Cat# 550261, RRID:AB_398460
Anti-CD11c FITC	BD Biosciences	Cat# 557400, RRID:AB_396683
Anti-CD45 Alexa Flour 700	eBioscience	Cat# 56-0451-82, RRID:AB_891454
Anti-CD11b APC-Cy7	BD Biosciences	Cat# 557657, RRID:AB_396772
Anti-CD11b Alexa Flour 700	Biolegend	Cat# 101222, RRID:AB_493705
Anti- MHC Class II (I-A/I-E) eFluor 450	eBioscience	Cat# 48-5321-82, RRID:AB_1272204
Anti-F4/80 BV650	Biolegend	Cat# 123149, RRID:AB_2564589
Anti-CD206 PE	Biolegend	Cat# 141706, RRID:AB_10895754
Anti-CD206 Alexa Flour 647	Biolegend	Cat# 141712, RRID:AB_10900420
Anti- Ki67 FITC	eBioscience	Cat# 11-5698-82, RRID:AB_11151330
Anti-CD62L Percp-Cy5.5	eBioscience	Cat# 45-0621-82, RRID:AB_996667
Anti-PD-1 PE-Cy7	eBioscience	Cat# 25-9985-82, RRID:AB_10853805
Anti-Foxp3 APC	eBioscience	Cat# 17-5773-82, RRID:AB_469457
Anti-Foxp3 FITC	eBioscience	Cat# 11-5773-82, RRID:AB_465243
Anti-CD44 APC-Cy7	Biolegend	Cat# 103028, RRID:AB_830785
Anti-CD44 V450	BD Biosciences	Cat# 560451, RRID:AB_1645273
Anti-Thy1.1 APC	BD Biosciences	Cat# 561409, RRID:AB_10683163
Anti-T-bet Percp-Cy5.5	eBioscience	Cat# 45-5825-82, RRID:AB_953657
Anti-CD3 Percp-Cy5.5	BD Biosciences	Cat# 561108, RRID:AB_10562558
Anti-CD3 APC-Cy7	BD Biosciences	Cat# 557596, RRID:AB_396759
Anti-IFNg Percp-Cy5.5	eBioscience	Cat# 45-7311-82, RRID:AB_1107020
Anti-TNFa PE-Cy7	BD Biosciences	Cat# 557644, RRID:AB_396761
Human Anti-Granzyme B PE-Texas Red	ThermoFisher Scientific	Cat# GRB17, RRID:AB_1500187
Human Anti-CD3 PE-Texas Red/ECD	Beckman Coulter	Cat# IM2705U, RRID:AB_130860

REAGENT or RESOURCE	SOURCE	IDENTIFIER
Human Anti-CD4 Percp-Cy5.5	eBioscience	Cat# 45-0048-42, RRID:AB_10804390
Human Anti-CD56 PE-Cy7	BD Biosciences	Cat# 335809, RRID:AB_399984
Human Anti-CD8a Pacific Blue	BD Biosciences	Cat# 558207, RRID:AB_397058
Human Anti-CD4 APC-Cy7	ThermoFisher Scientific	Cat# A15453, RRID:AB_2534466
Chemicals, Peptides, and Recombinant Proteins		
GMSCF	Preprotech, Inc	Cat# 315-03
PMA	Sigma-Aldrich	Cat# P8139
Ionomycin	Sigma-Aldrich	Cat# I0634
Monensin	Sigma-Aldrich	Cat# M5273
Brefeldin A	BD biosciences	Cat# 555029
TRIzol Reagent	Invitrogen	Cat# 15596018
Annexin V - PE	eBioscience	Cat# 556421
Annexin V binding buffer	eBioscience	Cat# 556454
Caspase 3/7 green	ThermoFisher Scientific	Cat# C10423
Fixable Viability Dye eFluor 506	ThermoFisher Scientific	Cat# 65-0866-14
Percoll	Cytiva (GE Healthcare)	Cat# 17089101
Cellstripper	Corning	Cat# 25-056-CI
Foxp3 / Transcription Factor Staining Buffer Set	eBioscience	Cat# 00-5523-00
ACK lysing Buffer	Lonza	Cat# 10-548E
Experimental Models: Cell Lines		
B16F10	I. Fidler (MD Anderson)	N/A
MC38	Kerafast, Inc.	Cat# ENH204-FP
B16F10 Sting$^{-/-}$	Generated in lab	N/A
Experimental Models: Organisms/Strains		
Mouse; C57BL/6J	Jackson Laboratory	Stock # 000664
Mouse Pmel TCR transgenic	Bred in house	N/A
Mouse: Sting$^{gt/gt}$ (*Tmem173^{gt}*)	Jackson Laboratory	Stock # 017537
Oligonucleotides		
Arg1	ThermoFisher Scientific	Mm00475988_m1
CCL2 (MCP1)	ThermoFisher Scientific	Mm00436439_m1
CCL22	ThermoFisher Scientific	Mm00436439_m1
CD11b	ThermoFisher Scientific	Mm00434455_m1
CD206 (Mrc1)	ThermoFisher Scientific	Mm01329362_m1
CD4	ThermoFisher Scientific	Mm00442754_m1
CD8	ThermoFisher Scientific	Mm01182107_g1
GMCSF (CSF2)	ThermoFisher Scientific	Mm99999059_m1
CXCL12 (SDF1)	ThermoFisher Scientific	Mm00445552_m1

REAGENT or RESOURCE	SOURCE	IDENTIFIER
FAPα	ThermoFisher Scientific	Mm00484254_m1
FasL	ThermoFisher Scientific	Mm00438864_m1
Foxp3	ThermoFisher Scientific	Mm00475156_m1
GARP (Lrrc32)	ThermoFisher Scientific	Mm01273954_m1
Granzyme B	ThermoFisher Scientific	Mm00442834_m1
IDO	ThermoFisher Scientific	Mm00492586_m1
IFNβ	ThermoFisher Scientific	Mm00439552_s1
IFNγ	ThermoFisher Scientific	Mm00801778_m1
IL10	ThermoFisher Scientific	Mm00439616_m1
IL15	ThermoFisher Scientific	Mm00434210_m1
IL1α	ThermoFisher Scientific	Mm00439620_m1
IL1β	ThermoFisher Scientific	Mm00434228_m1
IL2	ThermoFisher Scientific	Mm00434256_m1
IL4Rα	ThermoFisher Scientific	Mm00439634_m1
IL6	ThermoFisher Scientific	Mm00446190_m1
CXCL10 (IP-10)	ThermoFisher Scientific	Mm00445235_m1
ItgaV	ThermoFisher Scientific	Mm01302428_m1
CCL8 (MCP-2)	ThermoFisher Scientific	Mm01297183_m1
MHC I	ThermoFisher Scientific	Mm01612247_mH
MHC II	ThermoFisher Scientific	Mm00439216_m1
CXCL9 (Mig)	ThermoFisher Scientific	Mm00434946_m1
CCL3 (MIP1a)	ThermoFisher Scientific	Mm00441258_m1
CCL4 (MIP-1b)	ThermoFisher Scientific	Mm00443111_m1
CXCL2 (MIP2a)	ThermoFisher Scientific	Mm00436450_m1
PDL1	ThermoFisher Scientific	Mm00452054_m1
Perforin 1	ThermoFisher Scientific	Mm00812512_m1
Rae1	ThermoFisher Scientific	Mm00558293_g1
CCL5 (Rantes)	ThermoFisher Scientific	Mm01302428_m1
STAT1	ThermoFisher Scientific	Mm00439518_m1
TGFβ1	ThermoFisher Scientific	Mm01178820_m1
TGFβ2	ThermoFisher Scientific	Mm00436955_m1
TGFβ3	ThermoFisher Scientific	Mm00436960_m1
TNFα	ThermoFisher Scientific	Mm00443258_m1
VEGF	ThermoFisher Scientific	Mm00437304_m1
Gapdh	ThermoFisher Scientific	Mm99999915_g1
Actb	ThermoFisher Scientific	Mm00607939_s1
Software and Algorithms		
Prism 7	GraphPad Software, LLC (online download)	https://www.graphpad.com/scientific-software/prism/
FlowJo v.10	FlowJo, LLC (online download)	https://www.flowjo.com/solutions/flowjo/downloads

REAGENT or RESOURCE	SOURCE	IDENTIFIER
Microsoft Excel	Microsoft Inc	N/A
Microsoft Word	Microsoft Inc	N/A
Microsoft Powerpoint	Microsoft Inc	N/A
Other		
MACS LS columns	Miltenyi Biotech	Cat# 130-042-401
MidiMACS Separator	Miltenyi Biotech	Cat# 130-042-302
MACS MultiStand	Miltenyi Biotech	Cat# 130-042-303
Animal X-ray irradiator	Precision X-Ray	Model: X-RAD 320
Biomark HD system	Fluidigm	Cat# BMKHD
48.48 Dynamic Array IFC	Fluidigm	Cat# BMK-M-48.48